AD-A188 989 PHOTOENHANCED ATTACHMENT FOR OPTICAL CONTROL OF DIFFUSE 1/1
DISCHARGES(U) OREGON UNIV EUGENE J T MOSELEY ET AL
31 DEC 87 ARO-21849 5-PH DAAG29-84-K-0205

UNCLASSIFIED F/G 20/9 NL

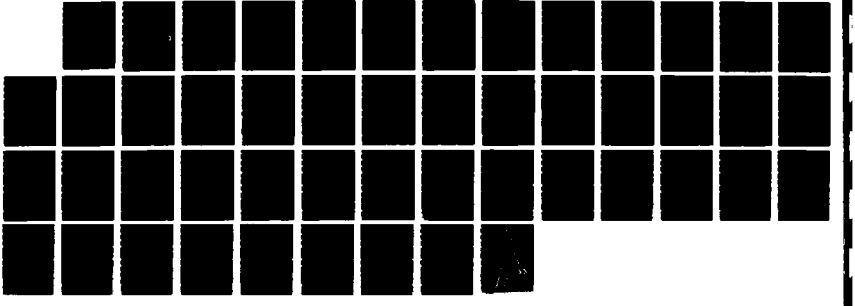

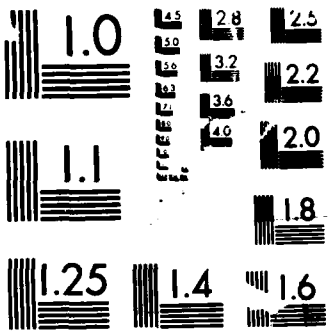

MICROCOPY RESOLUTION TEST CHART
NS-1963-A

UNCLASSIFIED
SECURITY CLASSIFICATION OF THIS PAGE (When Data Entered)

AD-A188 989

REPORT DOCUMENTATION PAGE

READ INSTRUCTIONS BEFORE COMPLETING FORM

1. REPORT NUMBER: ARO 21849.5-PH	2. GOVT ACCESSION NO.: N/A
3. RECIPIENT'S CATALOG NUMBER: N/A	
4. TITLE (and Subtitle): Photoenhanced Attachment for Optical Control of Diffuse Discharges	5. TYPE OF REPORT & PERIOD COVERED: Final, 1 Sept 84 - 31 Oct 87
	6. PERFORMING ORG. REPORT NUMBER:
7. AUTHOR(s): J. T. Moseley, J. L. Hardwick	8. CONTRACT OR GRANT NUMBER(s): DAAG-29-84-K-0205
9. PERFORMING ORGANIZATION NAME AND ADDRESS: University of Oregon, Eugene, OR 97403-1274	10. PROGRAM ELEMENT, PROJECT, TASK AREA & WORK UNIT NUMBERS:
11. CONTROLLING OFFICE NAME AND ADDRESS: U. S. Army Research Office, Post Office Box 12211, Research Triangle Park, NC 27709	12. REPORT DATE: 31 Dec 87
	13. NUMBER OF PAGES: 17
14. MONITORING AGENCY NAME & ADDRESS (if different from Controlling Office):	15. SECURITY CLASS. (of this report): Unclassified
	15a. DECLASSIFICATION/DOWNGRADING SCHEDULE:

16. DISTRIBUTION STATEMENT (of this Report)

Approved for public release; distribution unlimited.

17. DISTRIBUTION STATEMENT (of the abstract entered in Block 20, if different from Report)

NA

18. SUPPLEMENTARY NOTES

The view, opinions, and/or findings contained in this report are those of the author(s) and should not be construed as an official Department of the Army position, policy, or decision, unless so designated by other documentation.

19. KEY WORDS (Continue on reverse side if necessary and identify by block number)

Multiphoton ionization	sulfur dioxide
capture	ion
attachment	nitric oxide
detection	fluorobenzene

20. ABSTRACT (Continue on reverse side if necessary and identify by block number)

Production of negative ions has been identified in laser-generated plasmas containing nitric oxide, sulfur dioxide, or fluorinated benzenes. The mechanism for anion formation is assigned as dissociative attachment of photoelectrons to an excited electronic state of the parent molecule. Keywords:

DD FORM 1 JAN 73 1473 EDITION OF 1 NOV 65 IS OBSOLETE

UNCLASSIFIED
SECURITY CLASSIFICATION OF THIS PAGE (When Data Entered)

ARO 21849.5-PH

PHOTOENHANCED ATTACHMENT FOR OPTICAL CONTROL OF DIFFUSE DISCHARGES

FINAL REPORT

John T. Moseley
John L. Hardwick

31 December 1987

U.S. ARMY RESEARCH OFFICE

DAAG 29-84-K-0205

University of Oregon

Approved for public release; distribution unlimited

FINAL REPORT

Title: Photoenhanced Attachment for the Optical Control of Diffuse Discharges

Contract: DAAG 29-84-K-0205
Institution: University of Oregon
Authors: John T. Moseley
John L. Hardwick

Foreword

Although the formation of positive ions due to multiphoton excitation of low-pressure gases is a well documented phenomenon, and in many instances is well understood, virtually nothing is known about the formation of negative ions under similar conditions. The reason for this situation is not because of a lack of interest in negative ions; indeed, they are some of the most intensely studied species in molecular physics, and are responsible for a variety of physical and chemical phenomena. Rather, the failure to observe negative ions during multiphoton excitation is because their presence under such conditions seems, at first glance, quite implausible.

Negative ions are, in the gas phase, relatively fragile species. They are easily photodetached to form the corresponding neutral and low-energy electrons; and, since ion-ion neutralization reactions are extremely rapid, they will react readily with any positive ions which might be present. Moreover, to form them usually requires either high gas pressures (to promote three-body processes necessary for ordinary attachment) or moderate electron energies (to provide the 2-10 eV necessary

for dissociative attachment). Viewed with these criteria in mind, the typical multiphoton ionization environment might seem to be quite hostile to the generation and survival of negative ions.

We have observed as a part of this work the formation, under nearly collision-free conditions, of negative ions from a variety of precursors when irradiated using a tunable dye laser. These reactions involve precursors which were specifically chosen to have negligible dissociative attachment cross-sections for thermal electrons in the ground electronic state, and so they represent extremely unfavorable candidates for negative ion production when compared with molecules such as HI or O_3; nevertheless, we are able to detect the formation of negative ions with sufficient sensitivity to use both mass and wavelength resolution to study the processes responsible for their formation. We conclude that the most important such process is the dissociative attachment of low-energy electrons (typically less than 2eV) to molecules in excited electronic states.

Contents

Research Problem

The focus of this project has been to examine the physical and chemical behavior of small molecules in excited electronic states in the presence of thermal electrons. The motivation for this work was dictated by the known properties of negative ion formation in plasmas: since electron capture to form negative ions is responsible for plasma instabilities leading to reduced electron mobility in the plasma, these experiments point toward a simple and easily modeled method of using laser excitation of a diffuse discharge to control the bulk conductivity of the plasma, producing a simple, reliable, high-current optically controlled switch.

Major Results

During the present grant period, we have made the following accomplishments in pursuit of those goals:

1. We have discovered instances of dissociative attachment of photoelectrons which, because of the energetics of the species involved, we believe to be state-specific. This behavior was observed in NO, SO_2, and several fluorinated benzenes. These examples are described in more detail below, and we discuss the evidence that the electron attachment is to an excited electronic state of those molecules.

2. We have determined the specific channels of photodissociation and photoionization in carbon disulfide near 308 nm, demonstrating (a) that resonance enhanced features dominate the photoionization spectrum and (b) that

metastable states of CS are formed by excimer laser photolysis of the stable molecule CS_2. These metastable states, while not themselves appropriate for dissociative attachment of electrons, serve as prototypes for metastable radicals which will attach electrons. These experiments thus allow us detailed insight into the complex photophysical and photochemical processes surrounding laser excitation of stable small molecules which we expect to be important in laser excitation of plasmas in general. This work is described below and in the reprints appended to this report.

3. In work published during the current funding period but supported under the previous grant, we have determined the mechanism of photofragmentation of ferrocene, establishing the state distribution and kinetic energy of the fragmentation products when this important organometallic compound is photolyzed by an excimer laser. This work is described in the reprints appended to this report.

Experimental details

Briefly, this experiment involves allowing molecules to interact with laser radiation and low energy electrons in a low pressure reaction region at a constant electric potential. In practice, these electrons have been produced by the multiphoton ionization of part of the sample. A sample is introduced into the vacuum chamber using a pulsed valve with up to a 1 mm aperture and an open time of approximately 1 μsec. The backing

pressure is ordinarily less than 1 atm, so there is very little cooling of the sample during expansion; unnecessary cooling of the sample would lead to undesirable clustering, which would greatly complicate the interpretation of the results.

About 5 to 10 mm downstream from the nozzle, the sample is irradiated with the light from a tunable dye laser (Lambda Physik FL 2002) pumped by a XeCl excimer laser operating at 308 nm (Lambda Physik EMG 150). A variety of dyes were used, and the output of these dyes were doubled using an angle tuned extracavity doubling crystal for coverage through the visible and ultraviolet spectrum. The laser is directed into the sample chamber and loosely focused using either a long focal length lens or a reducing telescope. Power from the dye laser is typically 10 mJ/pulse in the fundamental and 1 mJ/pulse doubled.

The sample chamber was evacuated by a 6 inch oil diffusion pump with a refrigerated baffle to an ultimate pressure of 10^{-6} Torr; during the opening of the pulsed valve, the pressure rose to as much as $5x10^{-6}$ Torr. We were able to extract either positive or negative ions from the interaction region and focus them using cylindrical electrostatic lenses; these were then mass-analyzed using a quadrupole mass spectrometer and detected using an electron multiplier.

Current from the electron multiplier was measured using a gated integrator, and the output from the gated integrator was digitized and stored by a microcomputer for subsequent display and analysis. The same microcomputer also supervised other aspects of data acquisition such as tuning the dye laser and

doubling crystal, opening the gas nozzle, and firing the excimer laser.

We were able to confine free electrons to the interaction region by applying a weak magnetic field produced with a small solenoid surrounding this region. This technique, sometimes referred to as momentum filtering, was capable of preventing the electrons from leaving the interaction region while allowing more massive charged particles to pass through unimpeded. This arrangement allowed us to record a relatively weak signal from negatively charged ions without interference from the much stronger electron signal.

Dissociative attachment of electrons

Formation of atomic negative ions was observed in multiphoton excitation of nitric oxide, sulfur dioxide, and several fluorinated aromatic hydrocarbons. These will each be discussed in turn.

NO. Excitation of NO near 440 nm produces O^- at wavelengths corresponding to four-photon ionization of NO, while excitation near 226 nm produces O^- at wavelengths leading to two-photon ionization of NO. Both of these excitations involve the $A^2\Sigma^+$ electronic state of NO as an intermediate.

The spectrum of NO at 226 nm may conveniently be monitored either by measuring the electron current or by measuring the formation of O^- ions. A comparison of the signals recorded in these two ways reveals that the major features of the two spectra are identical; that is, O^- ions are produced whenever NO excitation through the $\underline{A}^2\Sigma^+$ state leads to ionization.

Four-photon ionization in NO is somewhat unusual, inasmuch as the strength of the ionization signal depends upon two resonances accidentally being excited by the same wavelength. Consequently, the line intensities have a characteristic 'signature' which is easily recognizable. Comparing the intensities of the multiphoton ionization lines with those of the O^- signal reveals a strong similarity between the two signals. Accordingly, we conclude that multiphoton ionization precedes negative ion formation.

The four-photon ionization of NO has been well-studied in this region. In particular, several different workers have resolved the energy of electrons ejected in the 455-390 nm interval [1,2]. There is a distribution of discrete electron energies produced, depending on the incident wavelength and the final state of the NO^+ ion, which ranges between 0 and 2 eV. Miller and Compton have performed a similar study involving the (1+1) photionization of NO at 226 nm, showing that the distribution of electron energies is almost identical.

The dissociative attachment of electrons to NO,

$$NO(X^2\Pi) + e^- \rightarrow N + O^- \qquad (1)$$

is endothermic by approximately 5 eV and so cannot proceed from ground state NO and 2 eV electrons. If the NO is present in the $A^2\Sigma^+$ state, however, the reaction becomes exothermic by approximately 0.45 eV, and we might expect thermal electrons to attach dissociatively:

$$NO^*(A^2\Sigma^+) + e^- \rightarrow N + O^- \qquad (2).$$

This situation is clouded somewhat by theoretical evidence

that an activation barrier exists for $NO(A^2\Sigma^+, \underline{v}=0)$, and electrons with energies over 1 eV may be required to produce dissociative attachment, depending on the details of the potential functions of NO and NO^-. Nonetheless, it is clear that electrons are produced with sufficient energy to overcome such a barrier, so that eq. (2) is reasonable from both energetic and kinetic points of view. We therefore regard photoenhanced dissociative attachement as the most plausible mechanism for producing O^- in the multiphoton excitation of NO.

C_6H_5F and related molecules. We have observed dissociative attachment of photoelectrons to four different fluorinated aromatic molecules, none of which are capable of dissociative attachment in the ground electronic state. These molecules, fluorobenzene and the three isomeric difluorobenzenes, all have strong electronic transitions between 275 and 260 nm, and it is this state which is being excited in the spectra we have observed. We easily observe the production of F^- ions in all of these molecules, and in some of the difluorobenzene isomers we observe other, more massive, negative ions being formed as well.

The interpretation of negative ion formation is most straightforward for fluorobenzene, for which the ionization potential and C-F bond strength are best known. The C-F dissociation energy for fluorobenzene is reported as 5.3 eV, a typical value for fluorocarbons. The electron affinity of fluorine is 3.4 eV, putting the threshold for dissociative attachment of electrons at 1.9 eV; this value is consistent with our observations of the onset of F^- production as a function of

the energy of incident electrons. The ionization potential of fluorobenzene is 9.2 eV, and the first allowed electronic transition falls at 264.4 nm (4.7 eV). Resonance-enhanced ionization through this transition is, therefore, a two photon process and will produce electrons with 0.2 eV kinetic energy or less. Dissociative attachment of electrons formed in this way to the ground state of fluorobenzene will therefore be an endothermic reaction, requiring about 1.7 eV of additional energy to proceed. We therefore interpret the formation of F^- ions as resulting from attachment of electrons to the excited electronic state, an exothermic reaction liberating approximately 3 eV excess energy.

Similar results are obtained in the three difluorobenzenes, leading us to conclude that the formation of F^- from excited states of fluorinated hydrocarbons may be of quite general occurrence. The principal ambiguity preventing the interpretation of the difluorobenzene experiments is, again, the uncertainty surrounding the energy of the photoelectrons produced. Recent two color spectroscopy on p-difluorobenzene has shown that thermal electrons are produced in quantity for a laser wavenumber of 36935 cm^{-1}, even though the region of greatest absorption is near 36840 cm^{-1}.

SO_2. We have identified formation of the sulfide ion, S^-, in the multiphoton excitation of sulfur dioxide using light from a xenon chloride excimer laser at 308 nm. This light populates the $^1A_2$ electronic state of SO_2, allowing that molecule to attach thermal electrons exothermically, producing S^- and O_2. Whether

this is the exact mechanism for producing S^- is uncertain, since a variety of additional products were observed in the positive and negative ion spectra. We are able, however, to establish S^- conclusively as a product of the excitation by monitoring the production of $^{34}S^-$ at its natural abundance of 4%. In addition, we have been able to monitor the production of S^- from excitation of SO_2 in the second spin-allowed band system near 220 nm.

Photoionization and photofragmentaion

In order to interpret the attachment of photoelectrons to small molecules, we required a greater insight into the details of the mechanisms by which those photoelectrons are produced.

CS_2. We have examined the production of photoelectrons and the attendant production of atomic and molecular ions from the multiphoton excitation of carbon disulfide in the range between 330 and 280 nm, covering much of the moderately strong $^1B_2$-$^1\Sigma_g^+$ band system. Although this molecular band system ultimately proved unsuitable for further study into optical switching, it provided a wealth of information regarding the mechanisms of ionization and dissociation in small molecules. Moreover, a study of this system allowed us to develop the methodology for examining the photophysics and photochemistry of other small molecules.

The experimental arrangement was much the same as that used to study negative ion formation, except that provision was made for introducing light from the excimer laser directly into the sample chamber. In this way, it was possible to control the wavelength of photolysis independent of the ionizing wavelength.

We have established in these experiments that, for this system, both fragmentation and ionization are important in determining the fate of the excited molecules and, thus, the composition of the laser-excited plasma. Fragmentation was found to precede ionization in every important instance, as demonstrated by the importance of resonance-enhanced ionization of the neutral fragments in the production of fragment ions. The neutral fragments are produced with internal excitation of up to 4 eV, accounting in some instances for virtually all of the excess energy of photolysis. In particular, all of the CS fragments we detected were formed in the metastable $\underline{a}^3\Pi$ state; this fact allowed us to probe the triplet manifold of that molecule in a way not previously possible, and allowed us to characterize a previously undiscovered triplet Rydberg state of CS. The deposition of energy into internal degrees of freedom is also reflected in the low translational energy of the neutral fragments as determined from the Doppler widths of their resonance-enhanced multiphoton ionization spectra. The details of these studies are described in more detail in two of the reprints appended to this report.

Ferrocene. In work supported by the previous grant and published during the current funding period, we have made a similar investigation of the multiphoton dissociation and ionization of ferrocene, $Fe(C_5H_5)_2$. The dynamics of this photodissociation are quite different, resulting in the liberation of substantial translational energy of the fragments. This disposition of energy has important consequences in the

photochemistry and multiphoton detection of ferrocene; this work is described in detail in two of the appended reprints.

References

1. J. Kimman, P. Kruit, and M. J. van der Wie, Chem. Phys. Lett. 88, 576 (1982).

2. J. C. Miller and R. N. Compton, J. Chem. Phys. 84, 675 (1986).

Publications

The following articles were published during the current funding period:

Y. Ono, J. L. Hardwick, and J. T. Moseley, "Multiphoton dissociation and ionization of CS_2 between 330 and 280 nm," J. Phys. Chem. 91, 4506-4510 (1987).

Y. Ono and J. L. Hardwick, "Resonance-enhanced multiphoton ionization detection of a new $^3\Sigma^+$-$\underline{a}\,^3\Pi$ band system in CS," J. Mol. Spectrosc. 119, 107-119 (1986).

H. T. Liou, P. C. Engelking, Y. Ono, and J. T. Moseley, "Atomic iron recoil in multiphoton dissociation of ferrocene," J. Phys. Chem. 90, 2892-2896 (1986).

H. T. Liou, Y. Ono, P. C. Engelking, and J. T. Moseley, "Two-color multiphoton dissociation and ionization of ferrocene," J. Phys. Chem. 90, 2888-2891 (1986).

The following conference presentations were made during the current funding period:

J. L. Hardwick, "Multiphoton photolysis and ionization of CS_2," Special Symposium on Lasers and Spectroscopy, University of Western Ontario, London, Ontario, Canada: June, 1986. (Invited paper)

J. L. Hardwick, Y. Ono, and J. T. Moseley, "Detection of CS_2 photodissociation products by resonance enhanced multiphoton ionization," Division of Chemical Physics, American Physical Society, University of Oregon, Eugene, Oregon: June, 1986.

J. L. Hardwick, Y. Ono, and J. T. Moseley, "Formation of O^- ions in the multiphoton excitation of NO," Forty-Second Symposium on Molecular Spectroscopy, The Ohio State University, Columbus, Ohio: June, 1987.

Personnel Supported

The following personnel were supported in part by this grant:

Dr. John T. Moseley
Dr. Yoshi Ono
Dr. John L. Hardwick
Dr. Timothy Steimle
Mr. Hui-Tarng Liou
Mr. Chie-Tong Kuo
Ms. Qi-Lin Wu

Mr. Liou received the Ph.D. in Physics in 1985. An abstract of his dissertation is appended to this report.

An Abstract of the Dissertation of

Huei-Tarng Liou for the degree of Doctor of Philosophy in the Department of Physics to be taken December 1985

Title: DYNAMICS OF MULTIPHOTON DISSOCIATION AND MULTIPHOTON IONIZATION

Approved: _____
Professor John T. Moseley

Multiphoton processes such as multiphoton dissociation (MPD) and multiphoton ionization (MPI) were investigated in a variety of molecules, including NO, the methylamines, and ferrocene. The primary purpose was to study the role of intermediate excited electronic states on the multiphoton process and on the products of MPD and MPI.

In the NO molecule, optical-optical doubly-resonant MPI was used to investigate the effect of accidental resonances in high-lying excited states.

Mass spectra of methylamine, dimethylamine, and trimethylamine were obtained by resonant MPI using a pulsed molecular beam source and the excimer laser wavelengths 193 and 248 nm. Power dependence measurements were made for the major fragment ions, and a rate equation model was employed to interpret the results. In cases where fragmentation was small, the mass resolved ions exhibited the expected

integral exponential power dependence; where fragmentation was extensive, non-integral power dependence was observed.

A single wavelength experiment at 447.6 nm and a two-wavelength experiment which used a fixed wavelength of either 248 or 350 nm in combination with a tunable dye laser (using Courmain C440 dye output wavelength from 438 to 457 nm) were used to investigate the dissociation mechanism of ferrocene. At 447.6 nm, the iron atom recoil in the MPD of ferrocene was investigated by monitoring the Doppler linewidth of the Fe MPI resonances. The iron atoms were observed to have a significant amount of translational energy, implying that the dissociation of ferrocene is through a non-concerted mechanism. In addition to ground state Fe, a high percentage of excited Fe atoms were produced by both the 248 nm radiation and the dye laser wavelengths. In contrast, 350 nm radiation did not significantly dissociate the ferrocene.

From the results of these experiments, it can be concluded that when a molecule is irradiated with visible/ultraviolet photons, the total energy of multiphoton absorption can significantly exceed that which is necessary for ionization or dissociation in the multiphoton absorption process, and whether a molecule undergoes ionization or dissociation is determined by the characteristics of the intermediate electronic states. The final products that result from multiphoton absorption are

also determined by the involvement of the intermediate excited electronic states in the process.

JOURNAL OF MOLECULAR SPECTROSCOPY 119, 107–115 (1986)

Resonance-Enhanced Multiphoton Ionization Detection of a New $^3\Sigma^+$–$a^3\Pi$ Band System in CS

Y. ONO AND J. L. HARDWICK

Department of Physics, University of Oregon, Eugene, Oregon 97403-1274

Resonance-enhanced multiphoton ionization has been used to detect absorption transitions from excited states of CS produced in the photolysis of CS_2. Transitions originating from the $a^3\Pi$ state of CS to a previously unobserved $^3\Sigma^+$ state. Rotational assignments for the (0,0), (1,0), (2,0), (0,1), and (0,2) bands have been made, the derived constants for those bands are used to characterize the CS molecule in this excited state, and the assumption that the upper electronic state is the $3s\sigma^3\Sigma^+$ Rydberg state is supported.

INTRODUCTION

Although the valence states of CS in the middle ultraviolet have been well studied (*1–3*), relatively little is known about the higher lying Rydberg states of this molecule. The only reported spectra of CS Rydberg states in the vacuum ultraviolet region were recorded at rather low resolution (*4*), and rotational fine structure has not been observed (*5*). The difficulty of obtaining spectra in this region is due in part to the stringent instrumental requirements of vacuum ultraviolet spectroscopy and in part to the fact that CS is not stable with respect to polymerization under ordinary conditions; it is usually prepared by photolysis of CS_2 or other thiocarbonyls, which themselves have strong spectra in the vacuum ultraviolet region.

Prinna and co-workers have predicted through SCF/CI calculations that the $3s\sigma^3\Sigma^+$ Rydberg state of CS will lie at about 61 000 cm^{-1} (*10*) and have calculated its bond length and vibrational force constant. This state will have a fully allowed transition from the lowest electronic state in the triplet manifold (the $a^3\Pi$ state), corresponding to the third positive group of CO. Since the $^3\Sigma^+$–$^3\Pi$ transition will fall near 35 000 cm^{-1}, which is a far more convenient region experimentally than is the vacuum ultraviolet, this band system seems the most promising way of studying the lowest triplet Rydberg state of CS.

As Black and co-workers have shown (*11*), photodissociation of CS_2 below 150 nm produces large quantities of CS in its $a^3\Pi$ state. By dissociating CS_2 with two photons having about the same total energy through the resonant $^1B_2$–$X^1\Sigma^+$ transition at 300 nm (*12*), we have produced a similar distribution of products (*13*). Thus, two-photon dissociation of CS_2 is an efficient method of preparing $a^3\Pi$ CS.

Several groups have reported mass-selected multiphoton ionization of small molecules. Although this method is ordinarily employed to study the mass spectrum of a particular parent at fixed discrete laser wavelengths, Morrison and Grant (*14*) have recently demonstrated that resonance-enhanced multiphoton ionization can also be

0022-2852/86 $3.00

used to record the optical spectrum of a particular fragmentation product, thus probing the nascent population distribution of that fragment.

We report in this paper the use of mass-selected resonance-enhanced multiphoton ionization spectroscopy to examine the spectrum of CS produced in the two-photon photolysis of CS_2 under nearly collision-free conditions. The only prominent spectrum in the region studied (265–309 nm) is due to a $^1\Sigma^+ - {}^1\Pi$ band system, which has been recorded at moderate resolution and rotationally analyzed. The upper $^1\Sigma^+$ electronic state exhibits all of the distinguishing features of the lowest Rydberg state predicted by Basua *et al.*

EXPERIMENTAL DETAILS

The experimental arrangement is similar to that described in a previous paper [2]. Light from a Lambda Physik EMG 102 excimer laser was split using an uncoated quartz window. Most of the excimer light passed through this window and was used to pump a grating-tunable dye laser (Lambda Physik FL 2002); the reflected part of the beam was focused into the sample compartment using a 10-cm-focal-length quartz lens. Frequency doubling the dye laser was accomplished with a temperature-stabilized angle-tuned KDP crystal (Lambda Physik FL30), and the fundamental was separated using a set of four Pellin–Broca prisms. The laser beam was narrowed spatially using a telescope and introduced into the sample chamber on the side opposite to the excimer beam, so that the two laser beams would be collinear and counterpropagating.

The sample of CS_2 was introduced into the vacuum chamber through a pulsed molecular beam valve (Lasertechnics 203LPV) with a 1-mm-diameter nozzle. The partial pressure of CS_2 on the high-pressure side of the valve was the room temperature vapor pressure of the liquid (ca. 400 Torr). Spectra were taken with argon and helium carrier gas at total pressures of up to 2 atm. The sample chamber was evacuated using a 6-in. oil diffusion pump with a refrigerated baffle. While pulsing, the pressure typically rose to about 5×10^{-6} Torr in the detection chamber. The background pressure was less than 10^{-6} Torr.

Ions produced by the laser were extracted, focused through a set of three cylindrical ion lenses, mass selected using a quadrupole mass filter, and detected with an electron multiplier. Detection was gated, with a typical detection window of 20 μsec.

Synchronization of the laser pulse, valve opening, and gated detection was accomplished using a dedicated microcomputer with an analog/digital conversion board controlling triggering circuits. A timing pulse from the computer triggered the valve, which then triggered a delay generator. The delay generator fired the excimer laser and triggered a second delay generator which, in turn, triggered the gated integrator which accumulated the ion signal. The microcomputer also supervised tuning the grating and doubling crystal for the dye laser as well as collecting and storing data for subsequent processing and analysis.

Wavelengths were recorded from the laser dial. These were calibrated using wavelengths of atomic sulfur transitions and were found to be in error by no more than 0.6 cm^{-1}, only slightly more than the nominal resolution of the frequency-doubled dye laser (0.3 cm^{-1}). We anticipate, then, that our systematic error of measurement between bands will ordinarily be less than 1 cm^{-1}, and within a short range will be less than 0.1 cm^{-1}.

[illegible] the experimental arrangement described [illegible] it was possible to monitor the production of CS^+ ions as a function of the wavelength of frequency-doubled radiation from the dye laser. If the dye laser was tightly focused into the sample volume, it was possible to produce CS^+ ions even with the excimer laser radiation blocked, i.e., the dye laser could be made to perform the multiple tasks of dissociating the parent CS_2, pumping the CS molecule from its ground state to the upper state, and ionizing the latter. The spectrum recorded in this way (Fig. 1a) was rather complicated and difficult to assign. The reason for this difficulty is that [illegible] the dye laser is tightly focused, it is capable of dissociating the CS_2 molecule and ionizing the CS fragment.

A much simpler spectrum was recorded (Fig. 1b) if only the light from the excimer laser was used to photolyze the sample and using a telescope to loosely focus the dye laser beam to excite the CS. We found it a simple matter to defocus the dye laser to the point where no CS^+ ions were formed with either of the exciting lasers blocked. With the light from the dye laser loosely focused in this way, it appears to serve only the function of exciting an electronic transition between discrete states of the nascent CS. The tasks of dissociating the CS_2 and ionizing the higher state of CS were left to the excimer laser.

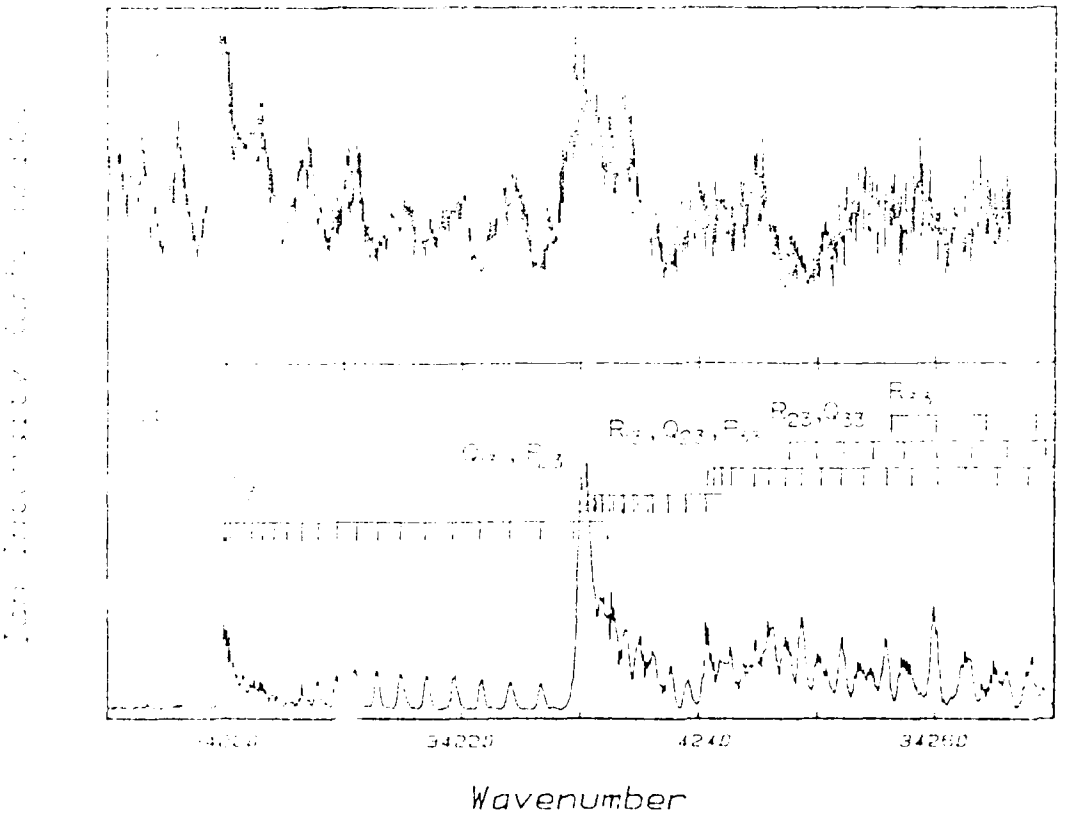

FIG. 1. Part of the multiphoton ionization spectrum of CS, recorded (a) using a single tightly focused beam from the dye laser to photolyze the parent CS_2 and ionize CS, and (b) using an excimer laser pulse to photolyze CS_2 while the loosely focused dye laser probes the transitions in CS (wavenumber scale is in cm^{-1}).

ANALYSIS

Appearance of the Spectrum

Four vibrational bands, all having much the same overall appearance, were observed in the two-color experiments. These bands are centered at about 2/3, 3/3, 2/1, and 3/2 cents.

The most conspicuous feature of the spectrum is that it is shaded to the violet. This fact immediately precludes the possibility that the spectrum belongs to any of the known systems of CS, as these are all shaded to the red. Furthermore, owing to the small rotational constant of the $X^1\Sigma$ electronic state of CS, it is also possible to assign a set of vibration transitions originating in the ground electronic state to any other known electronic state of CS.

The most notable feature of all of the observed spectra is the formation of sharp band heads. In each vibrational band, there are two sets of these heads with a spacing of about 70 to 100 cm^{-1} between adjacent members, corresponding to the spin-orbit coupling of the $a^3\Pi$ state (92.4 cm^{-1}). These features suggest that the $a^3\Pi$ state is involved in producing the spectrum; and, since the spectrum extends too far to the violet for the $a^3\Pi$ state to be the upper state, it must be the lower state. This inference is subsequently confirmed by vibrational and rotational analysis.

The third characteristic feature of the spectrum is a set of particularly simple and well-scattered branches which occur at the reddest edge of each of these bands (Fig. 1b). An examination of the wavenumber intervals between corresponding lines of

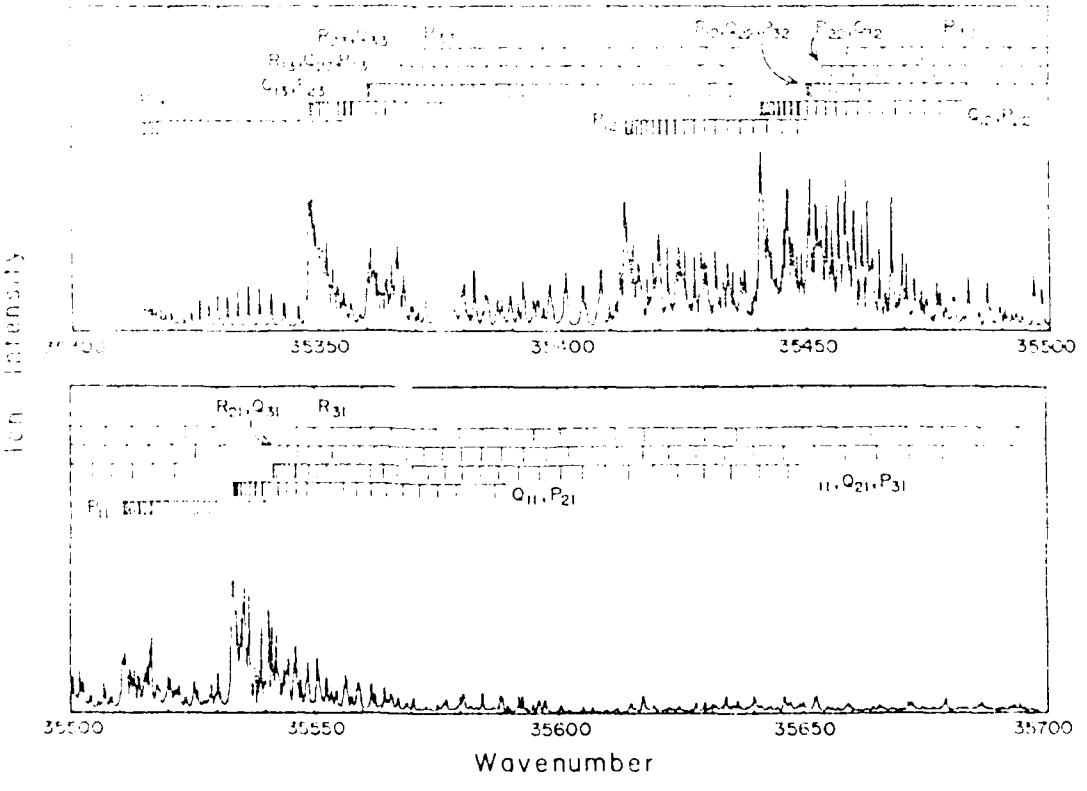

FIG. 2. The (0, 0) band of the $^3\Sigma^+$–$a^3\Pi$ system of CS (wavenumber scale is in cm^{-1}).

[illegible]

[illegible]

[illegible]

Neither spin–spin nor spin–rotation splitting was resolved. The value of D' determined from the rotational analysis was found not to be significantly different from the value determined from the vibrational frequency, assuming a harmonic oscillator approximation. The value of D' was therefore fixed at 1.8×10^{-6} cm^{-1}.

(2) The lines arising from F_1'' are not doubled, as would be expected if they arose from both parity components of the lower state. Instead, only a single parity component is represented in each branch: for the P_{11} branch, only the f component of the lower state was observed; for the P_{21} and Q_{11} branches, only the e component; and so on. The failure to observe Λ-type doubling in the F_1'' component implies that the excited state has $^3\Sigma$ symmetry, and the specific parity components which are observed identify it as a $^3\Sigma^+$ electronic state.

TABLE 1

[illegible]

J	P_{11}		Q_{11} P_{21}		R_{11} Q_{21} P_{31}		R_{21} Q_{31}		P_{31}		J
	calc	o-c	calc	o-c	calc	o-c	calc	o-c	calc	o-c	
1	[illegible]		[illegible]		[illegible]		36748.3	0.1	[illegible]		1
2	[illegible]		[illegible]	[illegible]	[illegible]	[illegible]	36751.[illegible]	[illegible]	[illegible]		2
3	[illegible]		[illegible]	[illegible]	[illegible]	[illegible]	[illegible]	[illegible]	[illegible]		3
4	[illegible]		[illegible]	[illegible]	[illegible]	[illegible]	[illegible]	[illegible]	[illegible]		4
5	[illegible]		[illegible]	[illegible]	[illegible]	[illegible]	[illegible]	[illegible]	[illegible]		5
6	[illegible]		[illegible]	[illegible]	[illegible]	[illegible]	[illegible]	[illegible]	[illegible]		6
7	[illegible]		[illegible]	[illegible]	[illegible]	[illegible]	[illegible]	[illegible]	[illegible]		7
8	[illegible]		[illegible]	[illegible]	[illegible]	[illegible]	[illegible]	[illegible]	[illegible]		8
9	[illegible]		[illegible]	[illegible]	[illegible]	[illegible]	[illegible]	[illegible]	[illegible]		9
10	[illegible]		[illegible]	[illegible]	[illegible]	[illegible]	[illegible]	[illegible]	[illegible]		10
11	[illegible]		[illegible]	[illegible]	[illegible]	[illegible]	[illegible]	[illegible]	[illegible]		11
12	[illegible]		[illegible]	[illegible]	[illegible]	[illegible]	[illegible]	[illegible]	[illegible]		12
13	[illegible]		[illegible]	[illegible]	[illegible]	[illegible]	[illegible]	[illegible]	[illegible]		13
14	[illegible]		[illegible]	[illegible]	[illegible]	[illegible]	[illegible]	[illegible]	[illegible]		14
15	[illegible]		[illegible]	[illegible]	[illegible]	[illegible]	[illegible]	[illegible]	[illegible]		15
16	[illegible]		[illegible]	[illegible]	[illegible]	[illegible]	[illegible]	[illegible]	[illegible]		16
17	[illegible]		[illegible]	[illegible]	[illegible]	[illegible]	[illegible]	[illegible]	[illegible]		17
18	[illegible]		[illegible]	[illegible]	[illegible]	[illegible]	[illegible]	[illegible]	[illegible]		18
19	[illegible]		[illegible]	[illegible]	[illegible]	[illegible]	[illegible]	[illegible]	[illegible]		19
20	[illegible]		[illegible]	[illegible]	[illegible]	[illegible]	[illegible]	[illegible]	[illegible]		20
21	[illegible]		[illegible]	[illegible]	[illegible]	[illegible]	[illegible]	[illegible]	[illegible]		21
22	[illegible]		[illegible]	[illegible]	[illegible]	[illegible]	[illegible]	[illegible]	[illegible]		22
23	[illegible]		[illegible]	[illegible]	[illegible]	[illegible]	[illegible]	[illegible]	[illegible]		23
24	[illegible]		[illegible]	[illegible]	[illegible]	[illegible]	[illegible]	[illegible]	[illegible]		24
25	[illegible]		[illegible]	[illegible]	[illegible]	[illegible]	[illegible]	[illegible]	[illegible]		25

J	P_{12}		Q_{12} P_{22}		R_{12} Q_{32} P_{32}		R_{22} Q_{32}		P_{32}		J
	calc	o-c	calc	o-c	calc	o-c	calc	o-c	calc	o-c	
1	[illegible]		36653.0		36654.7	0.0*	36658.0		36663.0		1
2	[illegible]		36651.5		36654.9	0.0*	36659.9		36666.6		2
3	[illegible]		36650.2		36655.2	0.0*	36661.9		36670.2		3
4	[illegible]		36649.0		36655.6	0.0	36664.0		36674.0	-0.4	4
5	[illegible]	0.0	36647.8		36656.2	0.1	36666.2		36677.9		5
6	[illegible]	-0.1	36646.8		36656.9	0.0	36668.6		36681.9	-0.2*	6
7	[illegible]	-0.1	36645.9		36657.5	0.0	36671.0	-0.3	36686.0	-0.2	7
8	[illegible]	-0.1	36645.1		36658.8	0.0	36673.5	-0.5	36690.2	-0.2	8
9	36631.1	-0.2	36644.4		36659.5	0.0	36676.2	-0.3	36694.6	0.0*	9
10	[illegible]	-0.1	36643.9		36660.6	0.0	36679.0	-0.4	36699.0	-0.2	10
11	36625.7	0.1	36643.4		36661.8	0.0	36681.8	-0.1*	36703.6	0.0	11
12	[illegible]	0.0	36643.1		36663.1	-0.2	36684.8	-0.2	36708.2		12
13	36622.8	0.1	36642.8		36664.5		36687.9	-0.2	36713.0		13
14	36621.9	0.1	36642.7		36666.1	-0.1	36691.1	-0.2	36717.8	-0.1	14
15	36619.3	0.3	36642.7	0.0[d]	36667.7		36694.4	-0.1*	36722.8	-0.3	15
16	36617.7	0.1	36642.7		36669.5		36697.9	-0.2	36727.9	-0.1	16
17	36616.2	0.2	36642.9		36671.3		36701.4	0.0	36733.1		17
18	36614.8		36643.2		36673.3		36705.0	0.0	36738.4		18
19	36613.6	0.2[d]	36[illegible].6		36675.4		36708.7		36743.8		19
20	36612.5		36[illegible].2		36677.6		36712.6		36749.3		20

J	P_{13}		Q_{13}		R_{13} Q_{23} P_{33}		R_{23} Q_{33}		R_{33}		J
	calc	o-c	calc	o-c	calc	o-c	calc	o-c	calc	o-c	
2	36559.6		36561.3	0.1	36564.7	0.1	36569.7		36576.4		2
3	36556.5		36559.9	0.1	36564.9	0.1	36571.6	0.3	36579.9		3
4	36553.5	0.0	36558.5	0.1	36565.2	0.2	36573.6	0.2	36583.6		4

*Blended line.
[d]Band head.

TABLE I—(Continued)

J	P_{11}		Q_{11} P_{21}		R_{11} Q_{21} P_{31}		R_{21} Q_{31}		R_{33}		J
	obs	o-c	calc	o-c	calc	o-c	calc	o-c	calc	o-c	
3	35521.4		35533.6		35547.5		35562.5		35579.9	0.2	8
4	35520.0	0.2	35533.4		35549.0		35565.8		35584.9	-0.2	9
10	35518.3	-0.4*	35533.4	0.0[a]	35550.7		35569.2		35589.[illegible]	-0.2	10
11	35516.6	0.0	35533.5		35552.6		35572.8		35595.2	-0.2	11
12	35515.4	0.0*	35533.9		35554.6	0.1*	35576.5		35600.7	-0.1*	12
13	35514.2	-0.1	35534.4		35556.6	0.0*	35580.4	0.4	35606.3	0.6	13
14	35513.2	0.0	35535.0		35559.2	0.0*	35584.5	0.2	35[illegible].2.1	-0.3	14
15	35512.3	0.0	35535.9		35561.8	0.2	35588.7	-0.3	35618.0	-0.5*	15
16	35511.6		35536.9		35564.5	0.2	35593.1	-0.2	35624.1	-0.4	16
17	35511.1		35538.1		35567.3	0.2	3[illegible]97.7	-0.2	35630.4	-0.4*	17
18	35510.7		35539.4	-0.1	35570.4	0.2*	35602.4	-0.2	35636.8	-0.4	18
19	35510.5		35540.9	-0.1	35573.6		35607.3	-0.2	35643.4		19
20	35510.5	0.2*	35542.6		35577.0	0.3	35612.4	-0.2	35650.2		20
21	35511.7		35544.4	-0.1*	35580.5	0.3	35617.6	-0.2*	35657.1		21
22	35511.0		35546.4	-0.1*	35584.2	0.5*	35623.0	-0.2	35664.2		22
23	35511.4		35548.6		35588.1	0.1	[illegible]628.6	-0.3	35671.5		23
24	35512.1		35550.9		35592.1	0.0	35634.3	-0.2	35678.9		24
25	35512.9		35553.4		35596.3	-0.1	35640.2	-0.2	35686.5		25
26	35513.9		35556.1		35600.7	-0.1*	35646.3	0.1	35694.2		26
27	35515.0		35[illegible]58.9		35605.2	-0.1	35652.4	0.2	35702.1		27
28	35516.3		35[illegible]61.9		35609.8	0.0	35658.6	0.3	35710.2		28
29	35517.7		35565.0		35614.7	0.1	35665.3	0.5	35718.4		29
30	35519.4		35568.3		35619.7	-0.1	35672.0	0.0	35726.8		30
31	35521.1		35571.8		35624.8	0.0	35678.9	0.4	35735.3		31
32	35523.1		35575.4		35630.2	-0.1*	35685.9	0.7	35744.0		32

(-O)

J	P_{12}		Q_{12} P_{22}		R_{12} Q_{22} P_{32}		R_{22} Q_{32}		R_{32}		J
	calc	o-c	calc	o-c	calc	o-c	calc	o-c	calc	o-c	
4	35434.5	-0.1	35444.6		35451.5		35460.0		35470.2		4
5	35436.8	-0.2	35443.7		35452.2		35462.4		35474.4		5

[illegible]

J	P_{12}		Q_{12} P_{22}		R_{12} Q_{22} P_{32}		R_{22} Q_{32}		P_{32}		J
	obs	o-c	obs	o-c	obs	o-c	obs	o-c	obs	o-c	
1	[illegible]		[illegible]		[illegible]		[illegible]	-0.2*	[illegible]		
2	[illegible]	[illegible]	[illegible]		[illegible]		[illegible]	0.0*	[illegible]	0.1*	2
3	[illegible]	0.1	[illegible]		[illegible]		[illegible]	0.2	35487.5	-0.1*	3
4	[illegible]	[illegible]	[illegible]		[illegible]	-0.2*	[illegible]	0.0	[illegible]	[illegible]	4
5	[illegible]	[illegible]	[illegible]		[illegible]	[illegible]	[illegible]	0.1	[illegible]	[illegible]	5
6	[illegible]	[illegible]	[illegible]		[illegible]	[illegible]	[illegible]	0.0*	[illegible]	[illegible]	6
7	[illegible]	[illegible]	[illegible]		[illegible]	[illegible]	[illegible]	0.0*	[illegible]	[illegible]	7
8	[illegible]	[illegible]	[illegible]		[illegible]	[illegible]	[illegible]	0.2	35512.0	[illegible]	8
9	[illegible]	[illegible]	[illegible]		[illegible]	[illegible]	[illegible]	0.1*	35513.0	[illegible]	9
10	[illegible]	[illegible]	[illegible]		[illegible]	-0.2*	35490.2	0.2	35518.0		10
11	[illegible]	[illegible]	[illegible]		[illegible]	-0.1*	35494.0	-0.4	35523.0		11
12	[illegible]		[illegible]	-0.1*	[illegible]	0.1	35498.0	-0.3	35529.9		12
13	[illegible]	[illegible]	[illegible]	0.0	[illegible]	0.0	35502.3	-0.2	35536.1		13
14	[illegible]	-0.1	[illegible]	0.1	[illegible]	0.0	35507.1	-0.1*	35541.1		14
15	[illegible]		[illegible]	0.3	[illegible]	0.2	35511.8		35547.3		15
16	[illegible]		[illegible]	0.1	35480.3	0.0	35516.1		35553.5		16
17	[illegible]		[illegible]	0.0	35483.5	0.0*	35520.8		35560.0		17
18	[illegible]		35449.0	0.1	35486.5	0.1*	35525.7		35566.5		18
19	35418.2	0.2*	35450.6	0.3	35489.8	0.0	35530.7		35573.2		19
20	35418.2		35452.4	0.1	35493.2	-0.2	35535.8		35580.0		20
21	35418.4		35454.3	0.1	35496.3	-0.2*	35541.1		35587.0		21
22	35418.8		35456.3	0.4*	35500.6	-0.1	35546.5		35594.1		22
23	35419.2		35458.5	0.2	35504.5	-0.3	35552.1		35601.4		23

J	P_{13}		Q_{13} P_{23}		R_{13} Q_{23} P_{33}		R Q_{33}		R_{33}		J
	calc	o-c	calc	o-c	calc	o-c	calc	o-c	calc	o-c	
2	35358.1		35356.6	0.0	35360.2	0.1*	35365.4		35372.2		2
3	35352.1		35355.5	0.0	35360.6	-0.3*	35367.4		35375.9		3
4	35349.1		35354.2	0.0	35361.1	0.3*	35369.6	-0.1	35379.8		4
5	35346.3	0.0	35353.1	0.1	35361.6	0.1*	35371.9	0.3*	35383.8	0.2	5
6	35343.6	-0.1	35352.1	0.1	35362.3	0.3	35374.3	0.0*	35387.9	0.1*	6
7	35341.0	-0.2	35351.2	0.0	35363.2	0.2	35376.8	0.0	35392.2	0.1*	7
8	35338.5	-0.1	35350.5	0.1	35364.1	0.1	35379.5	0.1	35396.5	-0.2	8
9	35336.2	-0.1	35349.8	0.1	35365.2	0.3	35382.2	0.1*	35401.0	0.1*	9
10	35333.9	0.1	35349.3	0.0	35366.3	0.2	35385.1	-0.1	35405.6	-0.4	10
11	35331.9	0.1	35348.9	0.1*	35367.6	-0.1*	35388.1	0.0	35410.3	-0.4	11
12	35329.8	0.0	35348.6	0.1*	35369.0	0.0	35391.2	0.0	35415.1		12
13	35327.9	0.2	35348.4		35370.6	0.1	35394.4	-0.2	35420.0		13
14	35326.2	0.0	35348.3	-0.3[a]	35372.2	-0.1	35397.8	0.0*	35425.1		14
15	35324.5	0.0	35348.4		35374.0	0.3*	35401.3	-0.2	35430.2		15
16	35323.0	0.0	35348.6		35375.9	0.1	35404.9	-0.4	35435.5		16
17	35321.6	0.1	35348.9		35377.9	0.2	35408.6	-0.4	35440.9		17
18	35320.4	0.2	35349.3		35380.0	0.0	35412.4	-0.3	35446.5		18
19	35319.2	0.1	35349.9		35382.3	0.0*	35416.3	-0.4	35452.1		19
20	35318.2	0.2	35350.6		35384.6	0.0	35420.4	-0.4	35457.9		20
21	[illegible]	0.2	35351.3		35[illegible]7.1	0.0	[illegible]	-0.3*	3.8		21
22	[illegible]	[illegible]	35352		[illegible]4.7	[illegible]	[illegible]	[illegible]	[illegible].8		22
23	[illegible]	[illegible]	35353.		[illegible]5.5	-0.2	[illegible]	[illegible]	[illegible]6.9		23
24	[illegible]5.6	0.2	35354.5		[illegible]6.5	-0.1	[illegible]7.		35462.1		24

(O-1)

J	P_{11}		Q_{11} P_{21}		R_{11} Q_{21} P_{31}		R_{21} Q_{31}		R_{31}		J
	calc	o-c	calc	o-c	calc	o-c	calc	o-c	calc	o-c	
4	34411.3		34415.5		34423.2		34430.8		34442.0	0.2*	4
5	34408.8		34414.7		34424.1		34433.5		34446.3	-0.2*	5
6	34406.5	0.1*	34414.1		34425.2		34436.3		34450.8		6

TABLE I (Continued)

J	P_{11}		Q_{11} P_{21}		R_{11} Q_{21} P_{31}		R_{21} Q_{31}		R_{31}		J
2	34434.1	0.0	34413.7		34396.0		34449.1	-0.1	34486.8	0.0	2
3	34427.3	0.1	34413.4		34399.2	0.0	34442.4	-0.2*	34480.4	-0.3*	3
4	34418.4	0.2	34411.7	0.1*	34401.8	0.2	34436.0	0.2*	34466.8	-0.1	4
5	34407.1	0.1*	34414.6		34407.5	0.2	34440.3	-0.1*	34470.7	-0.2*	5
6	34394.2	0.1	34418.8		34413.8	0.2	34446.1	-0.3*	34476.1	0.2	6
7	34379.8	0.1	34416.7		34421.7	0.2	34457.5	0.1	34481.7		7
8	34363.7	0.1	34418.1		34430.1	0.4*	34461.1	0.2	34487.8		8
9	34346.1	0.1	34419.2		34440.1	0.2	34468.3		34493.6		9
10	34326.4		34416.4		34445.4	0.1	34476.3		34498.3		10
11	34305.2		34413.2		34446.3	-0.3*	34471.9		34502.3		11
12	34282.6		34409.6		34445.1	-0.1*	34470.2		34512.5		12
13	34258.1		34421.1		34452.7	0.1*	34434.2		34519.2		13
14	34232.2	0.4	34422.2		34458.1		34489.4		34526.0		14

J	P_{12}		Q_{12} P_{22}		R_{12} Q_{22} P_{32}		R_{22} Q_{32}		R_{32}		J
	calc	o-c	calc	o-c	calc	o-c	calc	o-c	calc	o-c	
4	34407.5	0.2	34325.0		34331.8		34340.5		34350.6		4
5	34417.2	0.4	34324.1		34332.6	0.2	34342.8		34354.8		5
6	34411.8	0.1	34323.5		34333.5	0.1	34345.5		34359.1	-0.1	6
7	34404.2	0.0	34322.7		34334.6	0.1	34348.3		34363.6	-0.4	7
8	34395.3	-0.1	34322.3		34335.9	0.0	34351.3		34368.3	0.0	8
9	34385.1	-0.1	34322.0		34337.3	0.1	34354.4		34373.2	0.3*	9
10	34373.8	-0.1	34321.8	0.3*	34338.9	0.2	34357.7		34378.1	0	10
11	34361.2	-0.1	34321.9		34340.7	0.0	34361.1		34383.3	-0	11
12	34347.1	-0.1	34322.1		34342.5	0.1*	34364.7		34388.6	-0.4	12
13	34331.8	-0.4	34322.4		34344.6		34368.5	-0.1*	34394.0		13
14	34315.3	-0.2	34322.9		34346.8		34372.4	-0.1*	34399.7		14
15	34297.7	-0.1	34323.6		34349.2		34376.5	-0.2*	34405.4		15
16	34279.2	0.2	34324.4		34351.7	-0.4	34380.7	0.3*	34411.4		16
17	34259.1		34325.4		34354.4	-0.1	34385.1	0.1*	34417.5		17
18	34237.6		34326.6		34357.2	0.1	34389.6	0.1	34423.7		18
19	34214.7		34327.9		34360.2	0.0	34394.3		34430.1		19
20	34190.4		34329.3		34363.4	-0.1	34399.2		34436.6		20
21	34164.8	0.3*	34330.9		34366.7	-0.4	34404.2		34443.3		21
22	34137.7		34332.7		34370.2	-0.2*	34409.3		34450.2		22
23	34109.3		34334.6		34373.8		34414.7		34457.2		23
24	34079.5		34336.7		34377.6	0.0	34420.1		34464.4		24

J	P_{13}		Q_{13} P_{23}		R_{13} Q_{23} P_{33}		P_{23} Q_{33}		R_{33}		J
	calc	o-c	calc	o-c	calc	o-c	calc	o-c	calc	o-c	
3	34242.3		34235.7		34240.8	0.4	34247.6		34256.2		3
4	34243.4		34234.5		34241.8		34249.9	0.3*	34260.1		4
5	34238.4	0.1	34233.5		34242.0	-0.1	34252.2	-0.1*	34264.2		5
6	34234.2	0.2	34232.9		34242.6	0.0*	34254.7	-0.1	34268.4		6
7	34231.6	0.3	34232.8		34243.7	0.1	34257.3		34272.7		7
8	34229.2	0.2	34231.1		34244.7	0.1	34260.1		34277.2		8
9	34226.9	0.1	34230.6		34245.9	0.3	34263.0		34281.8		9
10	34224.8	0.1	34230.2		34247.3	0.1	34266.0		34286.5		10
11	34222.9	0.2	34229.9		34248.7	0.1	34268.2		34291.3		11
12	34221.1	-0.1	34229.8	0.2*	34250.3	-0.2	3427 .5		34296.3		12
13	34209.4	0.0	34229.8		34252.0	0.1*	3427 .9		34301.5		13
14	34207.8	-0.1	34230.0		34253.9	-0.3*	34279.4	0.0	34306.7		14
15	34206.4		34230.3		34255.9	0.0	34283.1	-0.2	34312.1		15
16	34205.1		34230.7		34258.0	-0.4*	34287.0	-0.7	34317.6		16
17	34204.0		34231.3		34260.2	-0.2*	34290.9	-0.3	34323.3		17
18	34203.0		34231.9		3 62.6	0.0*	34295.0	-0.2	34329.1		18
19	34202.1		34232.8		3 65.2		34299.2		34335.		19
20	34201.4		34233.7		3 67.8		34303.6		34341.0		20

TABLE 1.—*Continued*

J	P_{13}		Q_{13} P_{23}		R_{13} Q_{23} P_{33}		R_{23} Q_{33}		R_{33}		
	calc	o-c	calc	o-c	calc	o-c	calc	o-c	calc	o-c	
4	33126.4	0.1	33131.5		33138.3		33146.9		33157.1		4
5	33123.7	-0.1	33130.5		33139.1		33149.3		33161.3	0.0	5
6	33121.2	0.2	33129.7		33140.0		33151.9		33165.5	-0.1	6
7	33118.8	0.0	33129.0		33141.0		33154.6		33170.0	0.1*	7
8	33116.6	0.2	33128.5		33142.2		33157.5		33174.6	-0.1*	8
9	33114.5	-0.3	33128.1		33143.5		33160.5		33179.3	-0.2	9
10	33112.5		33127.9		33144.9	-0.2	33163.7		33184.2	0.0	10
11	33110.7		33127.8	0.0[a]	33146.6	-0.6	33167.0		33189.2	-0.3	11
12	33109.1		33127.9		33148.3		33170.5		33194.4	-0.2	12
13	33107.6		33128.1		33150.2		33174.1		33199.7		13
14	33106.2		33128.4		33152.3	0.0	33177.9		33205.1		14
15	33105.0		33128.9		33154.5	0.8*	33181.8		33210.7		15
16	33104.0		33129.6		33156.8	0.6*	33185.8		33216.5		16
20	33100.9	0.4[a]									

(3). The values of B' are quite similar to those found by Gauyacq and Horani (*17*) for the CS^+ ion in its $A^2\Sigma$ state, as would be expected for a Rydberg state of CS. We note with interest that the bond length we calculate from the rotational constants, r_0' = 1.5472 Å, agrees favorably with a bond length of 1.467 Å predicted by Bruna *et al.* (*10*) prior to the publication of the results of Gauyacq and Horani.

We conclude, therefore, that the transitions observed in this work belong to a $^3\Sigma^+ - a^3\Pi$ band system in CS, and that the upper state is most probably the $3s\sigma\,^3\Sigma^+$ Rydberg state predicted by Bruna *et al.* (*10*). From our assignments, we calculate T_e' = 62 074 cm^{-1} as the equilibrium energy of the upper state, compared with 61 209 cm^{-1} calculated by Bruna *et al.* The vibrational frequency of the upper state is about 10% less than that of the ion, which is not unreasonable for a Rydberg state.

There are two identifiable perturbations to the upper state, although such perturbations may be masked by our modest resolution. Our inability to resolve spin–splitting means that there is an intrinsic overlapping of several branches in each band. For example, the R_{11}, Q_{33}, and P_{33} branches will be exactly coincident in the case of vanishing spin–rotation and spin–spin coupling. In addition to this overlapping, there is considerable congestion near the center of the bands due to the collisions of lines from different branches (e.g., the R_{13} and R_{23} branches). A given spectral feature may thus have several assignments, and the strongest features are often actually blends of several rotational lines. Where this blending compromises our ability to measure a line position to better than 0.2 cm^{-1} relative to its neighbors, we have given the measurement a weight of zero in our fit; such assignments are denoted with an asterisk in Table I.

Rotational constants and upper state vibronic term values were determined from the measured line positions; these derived constants are collected in Table II. The errors on B' are determined by random errors of measurement within the band, whereas the errors on T_v' are due to systematic errors of calibration between bands; these errors are indicated in Table II. The rotational constant of the upper state was constrained to be the same for the (0, 0), (0, 1), and (0, 2) bands. In practice, since the data from the (0, 0) band were of higher quality than those from the other two, this meant that the upper state rotational constant B_0 was determined primarily from the (0, 0) band, and its value was held fixed for the (0, 1) and (0, 2) bands. The upper

TABLE II

Derived Constants for the $^3\Sigma$–$a^3\Pi$ Band System of CS

Band	T_v', cm^{-1}	B_v', cm^{-1}	$D_v' \times 10^{+6}$ cm^{-1}
(1,0)	64238.3(6)	0.83600(5)[b]	1.77[a]
(0,0)	63033.8(6)	0.85328(4)	1.77[a]
(0,1)	63033.5(6)	0.85328[a]	1.77[a]
(0,2)	63034.3(6)	0.85328[a]	1.77[a]

[a] Fixed.
[b] Error is one standard deviation in units of the last significant figure.

state term value T_0 was determined independently from the three bands. In the absence of [illegible] errors these values should have been within their mutual statistical [illegible] 0.05 cm^{-1}; in fact, the values varied by about 0.8 cm^{-1} between [illegible] lowest.

In addition to the lines listed in Table I, weak bandheads were found at 34 423 and 34 514 cm^{-1}. These were assigned to the Q_{11} and Q_{22} branches of the $(1, 2)$ band. These features were found to diminish in intensity with the addition of helium buffer gas, consistent with the assumption that $v'' = 2$ states of CS in $^3\Pi$ are formed largely from photolysis of "hot" bands of CS$_2$ at 308 nm. The additional cooling of the CS by the added buffer gas appears to depopulate the vibrationally excited states of CS to the extent that hot features in the CS fragment are less readily observed.

DISCUSSION

Although flash photolysis has been used for many years as an important spectroscopic tool in the study of free radicals in the gas phase, its use has mostly been confined to the study of photolysis products at thermal equilibrium. This restriction is due in part to the broadband flashlamps which have customarily been used for photolysis sources and in part to the inherent insensitivity of absorption spectroscopy, which is often the method of choice for detecting radicals. Furthermore, the very hot primary products produced by a conventional photolysis source often yield a spectrum far too complicated for convenient analysis. Finally, the difficulty of distinguishing the spectrum of the product from that of the parent is a recurring problem in the spectroscopy of free radicals. For these reasons, a study of the nascent product distribution in conventional flash photolysis is usually neither feasible nor informative, and so absorption spectra of free radicals in excited electronic states are not commonly observed.

The present method of recording the optical spectrum addresses many of these difficulties. Because the excimer laser is a relatively monochromatic photolysis source, the products are formed with a restricted range of excitation energies. Multiphoton ionization detection is intrinsically sensitive compared with absorption, and monitoring individual ions allows us to distinguish between the spectrum of the parent and that of the fragments without [illegible] loss of sensitivity.

The CS radical in its lowest triplet state has a chemical lifetime of several seconds and a radiative lifetime of several milliseconds. Since the laser pulses we used were of the order of 10^{-8} sec in duration, use of the technique we have described need not be restricted to such long-lived transients. Indeed, we expect this method could successfully be used for molecules with lifetimes as low as 10 nsec with no modification of our apparatus.

The main drawback to the use of multiphoton ionization for molecular optical spectroscopy is the problem of power broadening, which often limits the useful resolution to a value greater than the Doppler width. There is no general solution for this problem, only compromise between power broadening and signal strength on a case-by-case basis.

We have searched carefully for evidence of the $A^1\Pi$–$X^1\Sigma^+$ transitions reported by McCrary and co-workers in this region (*16*) and have found none. Although it is not possible to conclude on this basis that singlet states of CS are absent in our experiment, that inference is certainly plausible. If this is the case, the dominant steps in the dis-

ionization mechanism at this energy are likely to be quite different than the one proposed by McCrary *et al.* in the photoionization of Cs at 1543 nm. Instead, we posit the following primary steps to be the most important:

$$Cs(6s\,^2S_{1/2}) + 2h\nu \rightarrow Cs(n^2D_{3/2}) + e^- (5)$$

and

$$Cs(n^2D_{3/2}) + (CS_2, 2h\nu) \rightarrow Cs^+ + e^- \quad (6)$$

where $(CS_2, 2h\nu)$ is an undetermined electronically excited state of CS_2 formed by absorption of a second photon near 390 nm by the $^2D_{3/2}$ excited electronic state. Two-photon excitation of $Cs(6s\,^2S_{1/2})$ at 390 nm provides ~ exactly 2000 cm^{-1} more than the enhancement resonance necessary for the processes to be energetically possible.

ACKNOWLEDGMENT

This work was supported by the United States Army Research Office and a Grant-in-Aid from the Research Corporation.

RECEIVED: January 27, 1986

REFERENCES

1. R. W. FIELD AND T. BERGEMAN, *J. Chem. Phys.* **54**, 2936–2948 (1971).
2. G. W. TAYLOR, D. W. SETSER, AND J. A. COXON, *J. Mol. Spectrosc.* **44**, 108–117 (1972).
3. J. A. COXON, P. J. MARCOUX, AND D. W. SETSER, *Chem. Phys.* **17**, 403–415 (1976).
4. D. COSSART AND T. BERGEMAN, *J. Chem. Phys.* **65**, 5462–5468 (1976).
5. D. COSSART, M. HORANI, AND J. ROSTAS, *J. Mol. Spectrosc.* **67**, 283–303 (1977).
6. D. COSSART, *J. Phys.* **41**, 489–502 (1980).
7. T. BERGEMAN AND D. COSSART, *J. Mol. Spectrosc.* **87**, 119–195 (1981).
8. R. J. DONOVAN, D. HUSAIN, AND C. D. STEVENSON, *Trans. Faraday Soc.* **66**, 1–11 (1970).
9. S. BELL, T. NG, AND C. SUGGETT, *J. Mol. Spectrosc.* **44**, 267–278 (1972).
10. P. J. PRUNA, W. E. KAMMER, AND K. VASUDEVAN, *Chem. Phys.* **9**, 91–103 (1975).
11. G. BLACK, R. L. SHARPLESS, AND T. G. SLANGER, *J. Chem. Phys.* **66**, 113–2117 (1977).
12. CH. JUNGEN, D. N. MALM, AND A. J. MERER, *Canad. J. Phys.* **51**, 1471–1490 (1973).
13. Y. ONO AND J. L. HARDWICK, in press.
14. R. J. S. MORRISON AND E. R. GRANT, *J. Chem. Phys.* **77**, 5994–6004 (1982).
15. H. T. HOE, Y. ONO, P. C. ENGELKING, AND J. T. MOSELEY, *J. Phys. Chem.*, in press.
16. V. R. MCCRARY, R. LU, D. ZAKHEIM, J. A. RUSSELL, J. B. HALPERN, AND W. M. JACKSON, *J. Chem. Phys.* **83**, 3481–3490 (1985).
17. D. GALLAGHER AND M. HORANI, *Comm. At. Mol. Phys.* **56**, 585–600 (1978).

Reprinted from The Journal of Physical Chemistry, 1987, *91*, 4506.

Multiphoton Dissociation and Ionization of CS_2 between 330 and 280 nm

J. L. Hardwick,* Y. Ono, and J. T. Moseley

Chemical Physics Institute, University of Oregon, Eugene, Oregon 97403 *(Received: February 5, 1987; In Final Form: April 6, 1987)*

Products of the laser multiphoton dissociation of carbon disulfide have been studied by mass-selected resonance-enhanced multiphoton ionization spectroscopy between 330 and 280 nm. Photolysis is shown to produce CS in its $a^3\Pi$ state, atomic carbon in its ^3P, ^1D, and ^1S states, and sulfur in its ^3P, ^1D, and ^1S electronic states. The results indicate that fragmentation of CS_2 competes with ionization at moderate laser flux densities and that fragmentation typically precedes ionization in the formation of fragment ions. Doppler broadening measurements indicate that little of the excess energy of photolysis is released as translational energy.

Introduction

The single-photon photochemistry and spectroscopy of carbon disulfide are rich and varied, and this variety is reflected in the multiphoton processes it can undergo. In the near- and mid-ultraviolet, its absorption spectrum is dominated by exceedingly complicated transitions to electronic states derived from the $^1\Delta_u$ and $^1\Delta_u$ states of the linear molecule.[1-4] In the region between 150 and 200 nm the spectrum is less well understood, but there is clear evidence that both valence[5,6] and Rydberg[7,8] states are present.

The photochemistry of carbon disulfide is sensitive to the wavelength of photolysis. Absorption of a single photon at 193 nm excites the molecule to both singlet and triplet dissociative states, leading to production of $CS(X^1\Sigma^+)$ and sulfur atoms in the ^1D and ^3P states.[9-12] Further into the ultraviolet, production of $CS(a^3\Pi)$ becomes important; between 140 and 125 nm, CS is produced almost exclusively in the lowest triplet state.[13]

The multiphoton processes in CS_2 are even more diverse and are less clearly understood. Rianda et al.[14] studied the multiphoton ionization spectrum of CS_2 between 330 and 390 nm and reported the close similarity of the multiphoton ionization spectrum to the absorption spectrum over that range. They did not, however, analyze the products of the photolysis, monitoring instead the total ion current. Later, Seaver et al.[15] used mass spectrometry to analyze the products of multiphoton photolysis and ionization at 193 and 266 nm and concluded that two different mechanisms of ion formation operate at those two wavelengths. More recently, Fotakis et al.[16] reported formation of $CS(A^1\Pi)$ and $CS(d^3\Delta)$ in

(1) Jungen, Ch.; Malm, D. N.; Merer, A. J. *Chem. Phys. Lett.* **1972**, *16*, 302.
(2) Jungen, Ch.; Malm, D. N.; Merer, A. J. *Can. J. Phys.* **1973**, *51*, 1471.
(3) Hallin, K.-E. J.; Malm, D. N.; Merer, A. J. *J. Mol. Spectrosc.* **1975**, *54*, 318.
(4) Kleman, B. *Can. J. Phys.* **1964**, *41*, 2034.
(5) Douglas, A. E.; Zanon, I. *Can. J. Phys.* **1964**, *42*, 627.
(6) Desiderio, R. A.; Gerrity, D. P.; Hudson, B. S. *Chem. Phys. Lett.* **1985**, *115*, 29.
(7) Price, W. C.; Simpson, D. M. *Proc. R. Soc. London, Ser. A* **1938**, *169A*, 501.
(8) Greening, F. R.; King, G. W. *J. Mol. Spectrosc.* **1976**, *59*, 312.
(9) Yang, S. C.; Freedman, A.; Kawasaki, M.; Bersohn, R. *J. Chem. Phys.* **1980**, *72*, 4058.
(10) McCrary, V. R.; Lu, R.; Zakheim, D.; Russell, J. A.; Halpern, J. B.; Jackson, W. M. *J. Chem. Phys.* **1985**, *83*, 3481.
(11) Dornhöfer, G.; Hack, W.; Langel, W. *J. Phys. Chem.* **1984**, *88*, 3060.
(12) Kolbe, W. F.; Leskovar, B. *J. Chem. Phys.* **1986**, *85*, 7117.
(13) Black, G.; Sharpless, R. L.; Slanger, T. G. *J. Chem. Phys.* **1977**, *66*, 2113.
(14) Rianda, R.; Moll, D. J.; Kuppermann, A. *Chem. Phys. Lett.* **1980**, *73*, 469.
(15) Seaver, M.; Hudgens, J. W.; DeCorpo, J. J. *Chem. Phys.* **1982**, *70*, 63.

0022-3654/87/2091-4506$01.50/0

the multiphoton photolysis of CS_2 with a narrowed KrF laser operating near 248 nm. Bieniak and Ernst[17] have reported observations of multistep ionization in CS_2 at 337 nm involving both optical and collisional excitation.

The difficulty in interpreting the above multiphoton experiments, all of which use a fixed-wavelength laser, is that there is no obvious way of determining whether the results presented are characteristic of a broad wavelength range or, instead reflect local anomalies in the spectroscopy of CS_2 or its fragments. In this paper, therefore, we systematically examine the multiphoton spectrum of CS_2 over the wavelength range of its first strong absorption in the ultraviolet. Our goal is to identify the principal fragments produced in the multiphoton dissociation of carbon disulfide in the region between 330 and 280 nm using the mass-analyzed multiphoton ionization spectra of the parent CS_2 and its various fragments.

In doing so, we can demonstrate the importance of resonance effects not only in the formation of the CS_2^+ ion but also in the ionization of CS, C, and S fragments. The mass- and frequency-resolved spectra lead us to conclude that, to a good approximation, fragmentation precedes ionization in most instances at these wavelengths; that CS is produced in the $a^3\Pi$ state by a two-photon process at wavelengths near 308 nm; and that C and S atoms are produced both in ground and excited states with energies up to 3 eV.

Experimental Section

The experimental apparatus consists of a pulsed molecular beam (Lasertechnics LPV) with a 1-mm nozzle aperture, crossed at a distance 20–50-mm downstream with the output of a frequency-doubled Lambda Physik dye laser (FL2002E) pumped by a Lambda Physik XeCl excimer laser (EMG102). Ions created in the interaction region are extracted through a set of ion lenses, mass selected with a quadrupole, and detected with an electron multiplier. The chamber is pumped by a 6-in. oil diffusion pump and maintained at a pressure of less than 10^{-5} Torr during the experiment.

The excimer laser produces pulses of about 20-ns duration. The energy of the doubled dye laser pulse is typically 1 to 2 mJ, giving a mean pulse power near 100 kW. This was focussed by a 20-cm focal length lens.

Most spectra were recorded with a spectral line width of 0.3 cm^{-1}, scanning the laser wavelength by tuning the dye laser diffraction grating and KDP doubling crystal (Lambda Physik FL30) simultanously. A few features were also recorded at higher resolution, tuning the diffraction grating and an intracavity etalon to cover a narrow spectral range. In the high-resolution mode, the intracavity etalon in the oscillator of the dye laser provided laser wavelengths with a line width of 0.05 cm^{-1}. The dyes used were Rhodamine 640, 610, and 590 and Coumarin 540A. Some atomic and molecular resonant transitions were also probed with two-color multiphoton ionization, in which case part of the excimer laser beam at 308 nm was diverted and introduced into the chamber collinear and counterpropagating with respect to the dye laser beam.

The carbon disulfide was from MCB, Inc., and was used without further purification. The room temperature vapor pressure of CS_2 was introduced into the molecular beam valve with and without argon carrier gas. The ionization spectra did not change significantly under these conditions.

The laser pulse, valve opening, and gated detection were synchronized by a dedicated microcomputer with an analog/digital conversion board to control the various triggering circuits. A timing pulse from the computer triggered the valve, which in turn triggered a delay generator. The delay generator fired the excimer laser and triggered a second delay generator which, in turn, triggered the gated integrator to accumulate the ion signal. The microcomputer also supervised tuning the grating, etalon, and doubling crystal for the dye laser, collecting and storing data, and processing and analyzing the data following the experiment.

Results and Discussion

Several ionic species, both atomic and molecular, were observed as products of multiphoton dissociation and ionization of CS_2. The formation of each ion was monitored as a function of wavelength, and the appearance spectrum of the ion could, in most instances, be identified with the optical spectrum of the parent neutral species. Monitoring the production of S^+, for example, provides a resonance-enhanced multiphoton ionization spectrum of the sulfur atom freshly produced by the dissociation of CS_2, while monitoring the current of CS^+ yields a spectrum of neutral CS.

A discussion of the various products will require some understanding of the thermodynamics of CS_2 and its fragments. Using the appearance potential of CS^+ from CS_2 (15.80 ± 0.03 eV)[18] and the known ionization potential of CS (11.335 eV),[19] we can deduce the dissociation energy of the SC–S bond (to produce CS and S in their ground states) as 4.46 ± 0.04 eV. Alternately, this dissociation energy can be derived from the appearance potential of S^+ from CS_2 (14.787 ± 0.004 eV)[20] and the ionization potential of atomic sulfur (10.360 eV)[21] as 4.427 ± 0.004 eV, or about 35 700 cm^{-1} (280 nm). Dissociation to ground-state sulfur ($^3P_2$) and ground state CS ($^1\Sigma^+$) from ground-state CS_2 ($^1\Sigma_g^+$) is not, however, a spin-allowed process; the first such allowed process, producing $CS(X^1\Sigma^+)$ and $S(^1D_2)$, requires an additional 10 193 cm^{-1} (1.26 eV). To produce $S(^1S_0)$ requires 22 180 cm^{-1}, or 2.75 eV, over production of $S(^3P_2)$.

CS_2^+. The CS_2^+ molecular ion was prominent in the mass spectrum at all wavelengths studied. In general, its formation appeared to be enhanced by the one-photon $^1B_2$–$^1\Sigma_g^+$ resonances of CS_2 between 330 and 280 nm, and a plot of the ion current as a function of wavelength is very similar to the single-photon absorption spectrum of CS_2. Direct formation of the CS_2^+ ion from CS_2 is a three-photon process, since the ionization potential of CS_2 is 10.08 eV.[22] The similarity of the three-photon ionization spectrum to the absorption spectrum suggests that only the first photon is in resonance; in particular, the D and E states near 8 eV appear unimportant in promoting the ionization.

The spectroscopy of CS_2 in the near-ultraviolet has been the subject of several analyses.[1-5] There are two important sets of electronic states giving rise to band systems between 270 and 400 nm. The $^3A_2$ electronic state, of which only the B_2 spin-electronic component has been rotationally analyzed, probably arises from the $^3\Delta_u$ electronic state of the linear molecule, while the corresponding $^1\Delta_u$ state of linear CS_2 gives rise to $^1B_2$ and $^1A_2$ electronic states of the bent molecule. The most intense band system in this wavelength range is the $^1B_2$–$X^1\Sigma_g^+$ system, which has been the subject of extensive investigation by Merer and co-workers.[2] As expected, the three-photon ionization spectrum is most strongly enhanced by one-photon resonances with this strong singlet–singlet system.

CS^+. By monitoring the production of CS^+ we are able, in principle, to detect either the resonance-enhanced multiphoton ionization spectrum of the neutral CS molecule or the fragmentation of the CS_2^+ molecular ion. In the 330–310-nm excitation region, this ion current is relatively weak, and its spectrum is much the same as that of the CS_2^+ ion. All processes except the absorption of the initial photon by CS_2 appear to be nonresonant, and so it is impossible based on present evidence to determine whether ionization precedes or follows fragmentation in this spectral region.

To the violet of about 308 nm, however, a much stronger and simpler spectrum begins to emerge. Part of this spectrum is

(16) Fotakis, C.; Zevgolis, D.; Efthimiopoulos, T.; Patsilinakou, E. *Chem. Phys. Lett.* **1984**, *110*, 73.
(17) Bieniak, B.; Ernst, K. *Appl. Phys. B* **1983**, *31*, 153.
(18) Ono, Y.; Linn, S. H.; Prest, H. F.; Gress, M. E.; Ng, C. Y. *J. Chem. Phys.* **1980**, *73*, 2523.
(19) Huber, K. P.; Herzberg, G. *Constants of Diatomic Molecules*; Van Nostrand-Reinhold: New York, 1979.
(20) Eland, J. H. D.; Berkowitz, J. *J. Chem. Phys.* **1979**, *70*, 5151.
(21) Kaufman, V. *Phys. Scr.* **1982**, *26*, 439.
(22) Tanaka, Y.; Jursa, A. S.; Leblanc, F. J. *J. Chem. Phys.* **1960**, *32*, 1205.

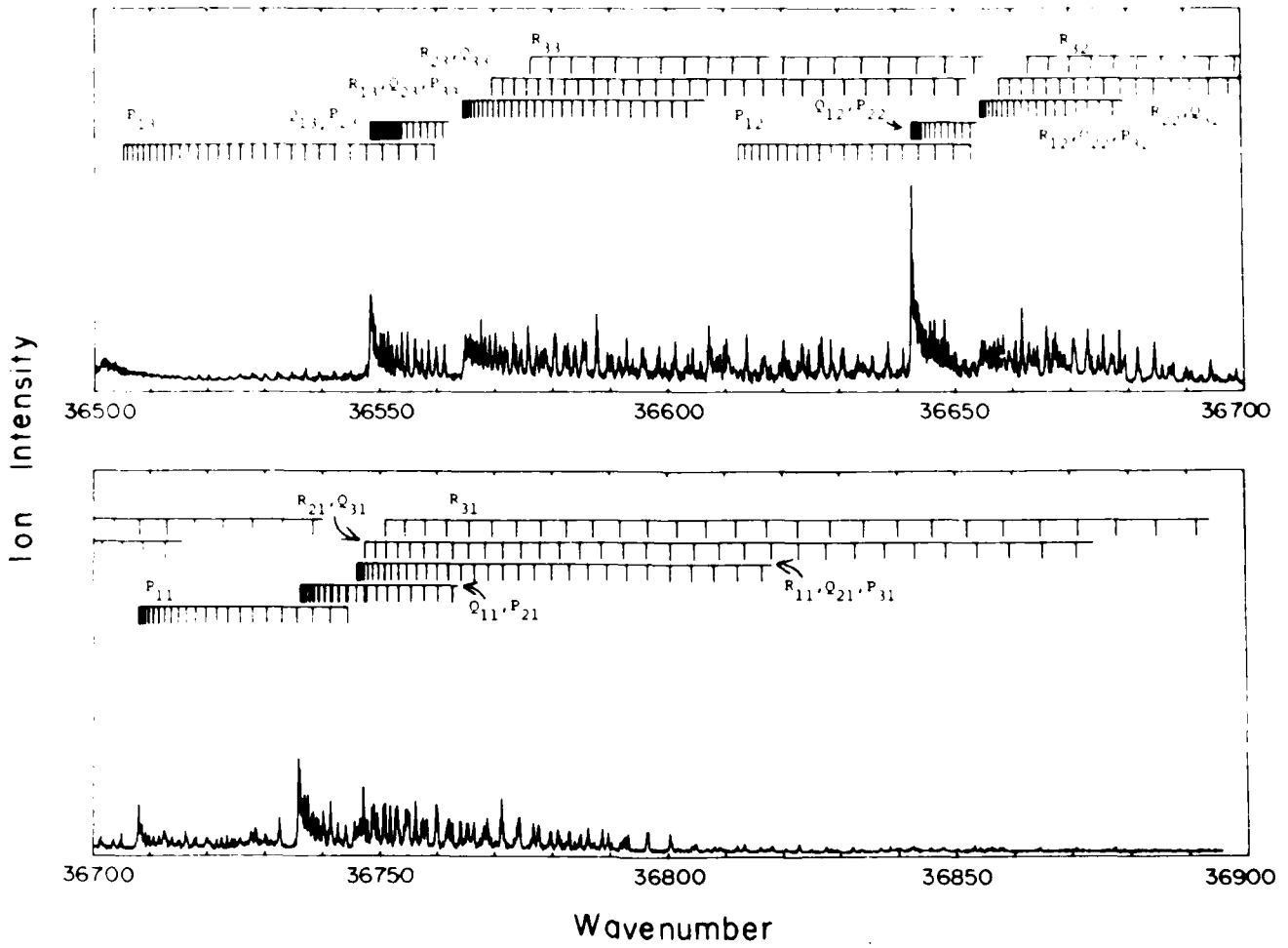

Figure 1. Part of the $^1\Sigma^+$–$a^3\Pi$ resonance-enhanced two-photon ionization spectrum of CS, recorded by monitoring the current of CS^+ as a function of laser wavelength. $CS(a^3\Pi)$ is produced from the photolysis of CS_2 by 308-nm excitation from a XeCl excimer laser. The wavenumber is given in cm^{-1}.

presented in Figure 1. This spectrum is dominated in this region by a one-photon resonance which is identified as a $^3\Sigma^+$–$a^3\Pi$ transition. The details of the vibrational and rotational analyses have been presented elsewhere[23] and will not be repeated here. All evidence points toward the direct production of $CS(^3\Pi)$ through the reaction

$$CS_2 \rightarrow CS(a^3\Pi) + S(^3P_{0,1,2}) \qquad (1)$$

This process requires 7.87 eV at threshold, or two photons at about 315 nm. Using the excimer laser at 308 nm for photolysis we would, therefore, expect the product $CS(a^3\Pi)$ to be formed with very little vibrational excitation. This is, indeed, what we observe; moreover, we find that using a relatively short-wavelength dye laser for photolysis produces many additional "hot" features in the spectrum of CS. Finally, we note that we observe the (1,2) band of this system upon photolyzing at 308 nm. Since there is not enough energy to produce $v'' = 2$ from ground state CS_2 at this wavelength, the band is presumably due to photolysis of hot CS_2. We find that by pressurizing the sample on the stagnation side of the nozzle with 2 atm of Ar we are able to cool the CS_2 vibrational energy sufficiently to discriminate against this band. We conclude that reaction 1 is, then, responsible for the direct production of CS in its lowest triplet state, and that the fragmentation of CS_2 to $CS(a^3\Pi)$ and $S(^3P_{0,1,2})$ competes with the ionization to CS_2^+ at the laser flux densities of this experiment.

S^+. Brewer et al.[24] have reported observing the $^3P_{0,1,2}$ and $^1D_2$ states of atomic sulfur as products of the photolysis of CS_2. In addition, we have been able to identify the $^1S_0 \rightarrow {}^3S_1$ transition in atomic sulfur. The wavelength of the atomic transitions we observe are summarized in Table I. The $3p^4\ ^3P_2 \rightarrow\rightarrow 4p\ ^3P_{0,1,2}$ lines appearing near 308 nm are of particular interest, since they fall within the gain profile of the 308-nm emission of the XeCl excimer laser and may be important in photochemistry promoted by that laser. Brewer et al.[24] remarked that these lines were far broader than they had expected and suggested that the additional line width might be due to Doppler broadening of translationally

TABLE I: Atomic Transitions Observed in the Multiphoton Dissociation and Ionization of CS_2

	assignment	ν_{obsd}	ν_{calcd}	$\nu_{obsd} - \nu_{calcd}$
S	$3p^4\ ^3P_0 \rightarrow\rightarrow 4p\ ^3P_0$	32 160.4	32 159.0	1.4
	$3p^4\ ^3P_0 \rightarrow\rightarrow 4p\ ^3P_2$	32 161.0	32 159.6	1.4
	$3p^4\ ^3P_1 \rightarrow\rightarrow 4p\ ^3P_1$	32 247.9	32 246.6	1.3
	$3p^4\ ^3P_1 \rightarrow\rightarrow 4p\ ^3P_2$	32 249.9	32 248.4	1.5
	$3p^4\ ^3P_2 \rightarrow\rightarrow 4p\ ^3P_0$	32 445.3	32 445.9	−0.6
	$3p^4\ ^3P_2 \rightarrow\rightarrow 4p\ ^3P_1$	32 444.2	32 444.6	−0.4
	$3p^4\ ^3P_2 \rightarrow\rightarrow 4p\ ^3P_2$	32 445.8	32 446.4	−0.6
	$3p^4\ ^1S_0 \rightarrow 4s\ ^3S^0$	33 149.9	33 150.8	−0.9
C	$2p^2\ ^3P_0 \rightarrow\rightarrow 3p\ ^3P_0$	35 677.3	35 676.3	1.0
	$2p^2\ ^3P_0 \rightarrow\rightarrow 3p\ ^3P_2$	35 693.8	35 692.7	1.1
	$2p^2\ ^3P_1 \rightarrow\rightarrow 3p\ ^3P_1$	35 675.2	35 674.2	1.0
	$2p^2\ ^3P_1 \rightarrow\rightarrow 3p\ ^3P_2$	35 685.7	35 684.5	1.2
	$2p^2\ ^3P_2 \rightarrow\rightarrow 3p\ ^3P_0$	35 655.5	35 654.6	0.9
	$2p^2\ ^3P_2 \rightarrow\rightarrow 3p\ ^3P_1$	35 661.9	35 660.8	1.1
	$2p^2\ ^3P_2 \rightarrow\rightarrow 3p\ ^3P_2$	35 672.0	35 671.0	1.0
	$2p^2\ ^1D_2 \rightarrow\rightarrow 3p\ ^1D_2$	31 207.9	31 209.0	−1.1
	$2p^2\ ^1D_2 \rightarrow\rightarrow 3p\ ^1S_0$	31 890.0	31 891.6	−1.6
	$2p^2\ ^1S_0 \rightarrow\rightarrow 5p\ ^1D_2$	31 874.6	31 875.9	−1.3
	$2p^2\ ^1S_0 \rightarrow\rightarrow 4p\ ^1S_0$	30 304.0	30 301.9	2.1

(23) Ono, Y.; Hardwick, J. L. *J. Mol. Spectrosc.* **1986**, *119*, 107.
(24) Brewer, P.; Van Veen, N.; Bersohn, R. *Chem. Phys. Lett.* **1982**, *91*, 126.

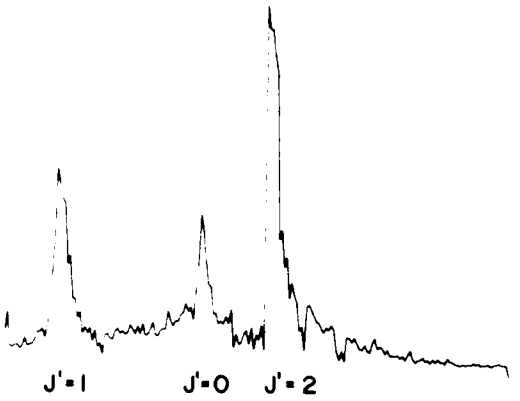

Figure 2. The spin components of the $^3P_2 \rightarrow \rightarrow {}^3P_{0,1,2}$ resonance-enhanced three-photon ionization spectrum of atomic sulfur, recorded by monitoring the current of S^+ as a function of laser wavelength. The spacing between the $J' = 1$ and $J' = 2$ components is 1.8 cm^{-1}, and the average line width (fwhm), which is power broadened by an undetermined amount, is 0.25 cm^{-1}. Wavenumbers of these transitions are listed in Table I.

hot sulfur atoms. Since we expect the majority of $3p^4\ ^3P$ sulfur atoms to be formed by the same reaction which produces $CS(a^3\Pi)$, and since that reaction is only slightly above threshold in this wavelength range, the mechanism of eq 1 is not consistent with a large Doppler broadening.

To clarify this issue, we have performed a series of measurements using an etalon-narrowed dye laser at several power levels. A typical scan at a low power level is shown in Figure 2. Experimenting with different power levels reveals that these lines are very sensitive to power broadening, and lowering the power to eliminate the effects of power broadening caused the signal/noise to deteriorate to unsatisfactory levels. That is, at power levels low enough to eliminate power-dependent broadening of the atomic lines, the signal is eliminated as well. Some asymmetric shifting due the ac Stark effect may also contribute to the observed line profiles; at the signal/noise level of our low power scans, it is not possible to distinguish these effects. Consequently, we are unable to establish the exact magnitude of the Doppler broadening, only to place an upper limit on its size. Nonetheless, based on measured line widths of 0.25 cm^{-1}, we can conclude that the translational energy is less than 0.3 eV. This result is consistent with a two-photon dissociation by the mechanism of eq 1 and is less than had been reported by Brewer et al.,[24] who were unable to resolve the $^3P_2 \rightarrow \rightarrow {}^3P_0$ spin component shown in Figure 2.

Some caution must be exercised in interpreting our observed line widths, since the photodissociation process need not produce isotropically distributed fragments. As a result, it would be unwise to attempt to extract a rigorous partitioning of the translational energy of the fragments without first determining whether there is any preferential direction of ejection of atoms with respect to the directions of propagation and polarization of the incident light.

Transitions originating in the ^1S and ^1D states of atomic sulfur have also been identified in the spectrum. These states of sulfur could be formed in two obvious ways: either from the dissociation of CS_2 or from the dissociation of CS. In order to form singlet sulfur from the dissocation of singlet CS_2, spin conservation requires that singlet CS be formed in the two reactions

$$CS_2 \rightarrow CS(X^1\Sigma^+) + S(^1D) \quad (2)$$

$$CS_2 \rightarrow CS(X^1\Sigma^+) + S(^1S) \quad (3)$$

We have searched carefully for evidence of the production of CS in its ground electronic state and have found none. We cannot, therefore, confirm the importance of reactions 2 and 3, and we conclude that formation of singlet states of atomic sulfur from the photodissociation of $CS(a^3\Pi)$ is equally plausible on the basis of our experimental results.

C^+. Our multiphoton ionization spectrum of atomic carbon is similar in many ways to that observed by Bolovinos et al., who identified the $^1D_2 \rightarrow \rightarrow 3p^1P_1$ transition in carbon produced from the photolysis of aromatic molecules,[25] and Whetten et al., who identified several transitions originating in the $^1D_2$ and $^3P_{0,1,2}$ levels of neutral carbon from photolysis of C_6F_6 and benzaldehyde.[26]

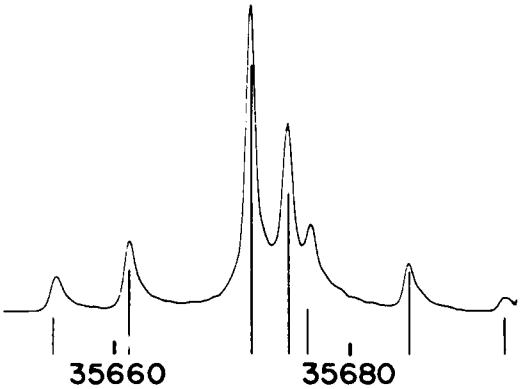

Figure 3. The $^3P_{0,1,2} \rightarrow \rightarrow {}^3P_{0,1,2}$ transition of atomic carbon, recorded by monitoring the current of C^+ as a function of laser wavenumber, which is given in cm^{-1} beneath the spectrum. The stick diagram below the experimental spectrum illustrates the intensity ratios for the spin components expected on the basis of the one-parameter model of ref 24, assuming equal population of the spin components of the lower state.

TABLE II: Intensity Factors for the Spin Components of a $^3P_J \rightarrow \rightarrow {}^3P_{J'}$ Two-Photon Transition

	$J' = 0$	$J' = 1$	$J' = 2$
$J'' = 0$	$^1/_9(1 + 2\epsilon)^2$	0	$^2/_9(1 - \epsilon)^2$
$J'' = 1$	0	$^1/_2(1 + \epsilon)^2 + \epsilon^2$	$^1/_2(1 - \epsilon)^2$
$J'' = 2$	$^2/_9(1 - \epsilon)^2$	$^1/_2(1 - \epsilon)^2$	$^4/_9(1 + {}^1/_2\epsilon)^2 + {}^1/_2(1 + \epsilon)^2 + 2\epsilon^2$

While it is not possible at this time to determine the exact partition of the remaining energy, we can rule out translational excitation of carbon atoms as being important. Upper limits to the Doppler widths of both the $2p^1D_2 \rightarrow \rightarrow 3p^1D_2$ and the $2p^1S_0 \rightarrow \rightarrow 5p^1D_2$ transitions have been measured, and both are found to be less than 0.3 cm^{-1}, which is only slightly above the Doppler width at room temperature. The most probable repository of the excess energy is, then, electronic excitation of one or both sulfur atoms to the $^1D_2$ state (1.15 eV).

Near 280 nm, we observe the $2p^3P_{J''} \rightarrow \rightarrow 3p^3P_{J'}$ transitions of the carbon atom, as shown in Figure 3. The intensities of these two-photon transitions are represented to a good approximation by the one-parameter model used by Brewer et al.,[24] reproduced here in Table II. Following those authors, we define an asymmetry parameter $\epsilon = [\beta(\pm 1)/\beta(0)]^{1/2}$, where $\beta(M_L)$ is the two-photon absorption cross section. We find that an adequate treatment of the observed intensities is provided by choosing an asymmetry parameter $\epsilon = 0.15$.

As expected, the $2p^3P_1 \rightarrow \rightarrow 3p^3P_0$ and $2p^3P_0 \rightarrow \rightarrow 3p^3P_1$ transitions are not observed. The $2p^3P_2 \rightarrow \rightarrow 3p^3P_0$ transition, which should have the same intensity as the $2p^3P_0 \rightarrow \rightarrow 3p^3P_2$ transition, is actually observed to be somewhat stronger; a similar disparity exists between the $2p^3P_2 \rightarrow \rightarrow 3p^3P_1$ and $2p^3P_1 \rightarrow \rightarrow$

(25) Bolovinos, A. Spyrou, S.; Cefalas, A. C.; Philis, J. G.; Tsekeris, P. *J. Chem. Phys.* **1986**, *85*, 2335.
(26) Whetten, R. L.; Fu, K.-J.; Tapper, R. S.; Grant, E. R. *J. Phys. Chem.* **1983**, *87*, 1484.

$3p^3P_2$ transitions. These slight enhancements of $J'' = 2$ relative to 0 and 1 may be a reflection of the population distribution within the $2p^3P_J$ states.

Conclusions

The multiphoton dissociation of CS_2 in the wavelength range from 330 to 280 nm is shown to produce carbon and sulfur atoms in their lowest three electronic states and CS in its lowest triplet state. The electronic excitation of the products amounts to as much as 2.7 eV for the atoms and over 3 eV for the CS fragment.

The atomic lines are all quite sensitive to power broadening and, possibly, the ac Stark effect, making accurate measurement of the line widths impossible in the present experiment. Upper limits for some Doppler widths have been measured, however, and these are only slightly greater than the room-temperature Doppler width. This leads us to conclude that little of the excess energy of photolysis is deposited as translational energy, but rather that most is taken up by internal degrees of freedom of the fragments.

Finally, we note that the resonance effects substantially change the distribution of product ions over the relatively narrow wavelength range we have investigated, and there is every reason to believe that the distribution would change even more drastically as other electronic states of CS_2 are probed. In particular, the production of S^+ is greatly enhanced near the 308-nm XeCl excimer band due to the two-photon $3p^4\ ^3P_J \rightarrow 4p\ ^3P_J$ transition in atomic sulfur, which is accidentally in resonance with the laser wavelength. We expect this resonance to play an important part in the multiphoton photolysis and ionization of many sulfur-containing compounds, and so would urge great care in the interpretation of such experiments.

Acknowledgment. This work was supported by the United States Army Research Office under Contract No. DAAG 29-84-K-0205.

Registry No. CS_2, 75-15-0; CS, 2944-05-0; C, 7440-44-0; S, 7704-34-9.

Reprinted from The Journal of Physical Chemistry, 1986, *90*, 2888

Two-Color Multiphoton Dissociation and Ionization of Ferrocene

H. T. Liou,† Y. Ono,* P. C. Engelking,* and J. T. Moseley

Departments of Physics and Chemistry, University of Oregon, Eugene, Oregon 97403
(Received: October 11, 1985)

The state distributions and relative yields of iron atoms generated in the multiphoton dissociation of ferrocene by the combined radiation of an excimer laser (248 or 351 nm) and a dye laser in the region 430–452 nm were probed by multiphoton ionization. The use of different wavelengths alters the amount of energy deposited in ferrocene prior to dissociation. Comparison of the two-color work with spectra obtained with purely visible radiation reveals that 351-nm radiation is ineffective in producing rapid dissociation, whereas 248 nm produces iron in a large number of electronic states. The rapid production of iron appears to require 1.5 eV of excess energy above the dissociation threshold and is likely a direct dissociation on a repulsive surface.

Introduction

The process of unimolecular dissociation has been well studied[1] and is very accurately characterized in many cases by RRKM theory[2] or quasiequilibrium theory[3] (QET). The work in this field has almost exclusively centered on single dissociation processes yielding two products. Often, the time-of-flight technique is employed to measure the velocity and mass of one of the products which, through conservation of momentum and energy, allows a measure of the kinetic energy release.[4,5] More recently, the statistical treatment of unimolecular dissociation has been extended to fragmentation processes yielding several products,[6] formulating the partitioning of excess energy into the available degrees of freedom[7] and identifying the experimentally observable[8] characteristics which can discriminate between sequential and simultaneous dissociation mechanisms.

In contrast to statistical decomposition, if dissociation occurs on a time scale that is fast compared to redistribution of energy among vibrational modes, dissociation may be highly specific in the resulting distribution of energy among degrees of freedom. Occasionally, this has been observed by chemical activation:

† Present address: Department of Chemistry, University of Pennsylvania, Philadelphia, PA 19104.

(1) Spicer, L. D.; Rabinovitch, B. S. *Annu. Rev. Phys. Chem.* **1970**, *21*, 349. Setser, D. W. *MTP Int. Rev. Sci. Phys. Chem.* **1972**, *9*, 1. Quack, M.; Troe, J. *Gas Kinetics and Energy Transfer*, Vol. 2, Ashmore, P. G., Donovan, R. J. Ed.; The Chemical Society: London, 1977; p 175. Quack, M.; Troe, J. *Int. Rev. Phys. Chem.* **1981**, *1*, 97. Holbrook, K. A. *Chem. Soc. Rev.* **1983**, *12*, 163. Kassel, L. S. *Kinetics of Homogeneous Gas Reactions*; Chemical Catalog Co.; New York, 1932.

(2) Marcus, R. A.; Rice, O. K. *J. Phys. Colloid. Chem.* **1951**, *55*, 94. Marcus, R. A. *J. Chem. Phys.* **1952**, *21*, 359.

(3) Vestal, M.; Wahrhaftig, A. L.; Johnston, W. H. *J. Chem. Phys.* **1962**, *37*, 1276.

(4) Franklin, J. L. *Science* **1976**, *193*, 725.

(5) Safron, S. A.; Weinstein, N. D.; Hershbach, D. R.; Tully, J. C. *Chem. Phys. Lett.* **1972**, *12*, 564. Farrar, J. M.; Lee, Y. T. *J. Chem. Phys.* **1976**, *65*, 1414.

(6) Silberstein, J.; Levin, R. D. *Chem. Phys. Lett.* **1980**, *74*, 6. Silberstein, J.; Levin, R. D. *J. Chem. Phys.* **1981**, *75*, 5735.

(7) Ohmichi, N.; Silberstein, J.; Levine, R. D. *Isr. J. Chem.* **1984**, *24*, 245.

(8) Bernstein, R. B. *J. Phys. Chem.* **1982**, *86*, 1178.

0022-3654/86/2090-2888$01.50/0

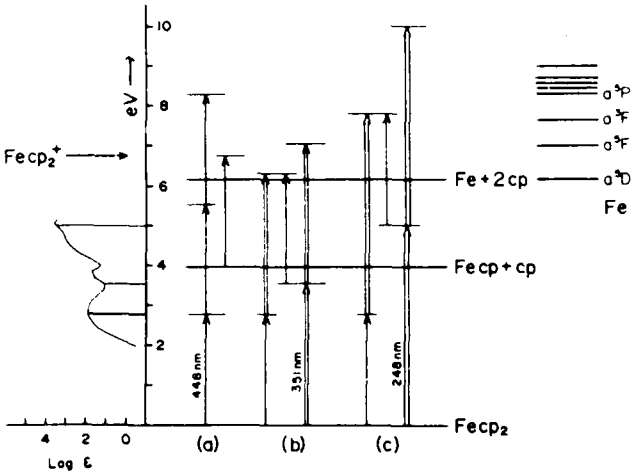

Figure 1. Various amounts of excess energy for dissociation of ferrocene are produced with different wavelengths, either singly or in combination. The absorption spectrum on the left shows allowed ferrocene transitions. (a) shows 2.1-eV excess energy is produced with 448 nm alone, (b) shows 0.7-eV excess is provided by 351-nm radiation, and (c) shows an ample 3.8 eV from two photons of 248-nm radiation.

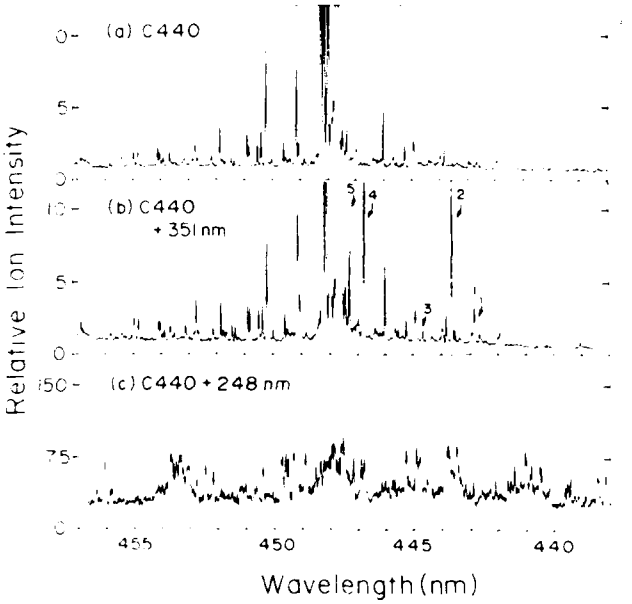

Figure 2. Multiphoton dissociation/multiphoton ionization spectra of ferrocene, using (a) C440 dye laser radiation alone, (b) C440 + 351 nm, (c) C440 + 248 nm. The wavelength is that of the C440 dye laser.

Rowland and co-workers[9] have observed rapid, nonstatistical dissociation of $Sn(CH_2CH{=}CH_2)_4$ or $Ge(CH_2CH{=}CH_2)_4$ upon addition of an F atom to the double bond, much faster than accountable by RRKM. More often, rapid, direct dissociation is observed in photofragmentation.[10]

These two mechanisms, one statistical, the other direct, apply to different molecules. A molecule as large as ferrocene (bis(cyclopentadienyl)iron) has two factors that would favor a statistical mechanism of photodissociation: (1) a large number of vibrational modes (57 internal degrees of freedom), and (2) a high density of electronic states of various multiplicities. It would seem that the great many vibrational modes would provide ample opportunity for mode coupling and would serve as a bath for quasiequilibrium to develop. The high density of electronic states would provide ample opportunity for curve crossings to prevent direct dissociation on an isolated electronic surface. The lack of phosphorescence in ferrocene[11] indicates ample intersystem conversion and relaxation even in energetically low-lying states; the situation would appear even more complicated near the dissociation threshold. From these considerations, it might be expected that ferrocene would be a typical example of statistical unimolecular decomposition.

The observation of iron atoms produced in high yields in multiphoton dissociation (MPD) of ferrocene, as detected by multiphoton ionization (MPI) near 300 nm, suggests that the mechanism for iron production via ferrocene decomposition is not simply statistical.[12] The appearance of iron within 1 ns, using 400-nm radiation,[13] also suggests that the energy is not randomized over all 57 internal degrees of freedom.

In a subsequent paper[14] we demonstrate a method for probing the resulting translational energy distribution for the product of a two-step dissociation process using a narrow-line-width tunable laser in the wavelength region 430–452 nm. The Doppler profile of some strong Fe lines resulting from the multiphoton dissociation of ferrocene reveals that a direct dissociation occurs and that most of the excess energy appears as translational energy of the products. In this paper, we examine the combined dye laser radiation with varying amounts of excimer laser radiation in order to investigate changes in the dissociation process, particularly the final electronic state of Fe, as a function of excess energy. We find that the rapid direct dissociation of ferrocene does not occur with 0.9-eV excess energy, proceeds rapidly with 2.1-eV excess energy, and not only proceeds rapidly with 3.8-eV excess energy, but also produces electronically excited iron in a variety of states.

The experimental MPD situations which we wish to investigate are illustrated in Figure 1. In (a), three photons of 448-nm radiation exceed the 6.2-eV dissociation threshold by 2.1 eV. In (b), the maximum available energy is 0.9 eV above the dissociation threshold. In (c), two 248-nm photons provide the excess 3.8 eV.

The iron product atoms will be probed by a dye laser operating near 448 nm. MPI resonances will allow us to determine what states of iron are produced.

Experiment

The experimental arrangement consists of an excimer laser, a dye laser,[15] and a parallel plate ionization chamber. A quartz beam splitter placed in the path of the excimer laser beam removes 8% of the UV radiation for delivery to the sample; the transmitted beam pumps the Coumarin 440 (C440) dye laser. The UV radiation passes through a variable attenuator assembly (a set of 20 removable quartz slide covers) and is combined coaxially with the dye laser beam by a high reflectance dielectric mirror. The UV radiation exposes a volume that totally includes that volume irradiated by the visible light. The beams are focussed by a 16-cm focal length quartz lens into the parallel-plate ionization chamber containing 7 mTorr of ferrocene (room temperature vapor pressure),[16] at a total pressure of 100 mTorr. Products of ferrocene dissociation are eliminated by maintaining a gentle flow of the background gas, slowly pumped over the ferrocene and through the chamber. A potential of approximately 250 V is applied across the plates and the total ionization signal is processed by a gated integrator and recorded by either a computer or a chart recorder. The laser powers were monitored separately with a Gentec Model Ed-100 power meter for the UV and an Analog Modules Inc., LEM 100 photodiode for the visible.

Studies of ion products were performed with a quadrupole mass spectrometer. In the static gas cell mode, ions created in the 7-mTorr region are extracted through a 1.5-mm-diameter aperature, mass analyzed with a quadrupole mass spectrometer, and detected with an ETP AEM-2000 electron multiplier. In a pulsed

(9) Rodgers, P.; Montague, D. C.; Frank, J. P.; Tyler, S. C.; Rowland, F. S. *Chem. Phys. Lett.* **1982**, *89*, 9. Rodgers, P.; Selco, J. I.; Rowland, F. S. *Chem. Phys. Lett.* **1983**, *97*, 313.
(10) Leone, S. R. *Adv. Chem. Phys.* **1982**, *50*, 255.
(11) Muller, L. A. *Ann Phys.* **1927**, *82*, 39.
(12) Engelking, P. C. *Chem. Phys. Lett.* **1980**, *74*, 207.
(13) Leutwyler, S.; Even, U.; Jortner, J. *Chem. Phys. Lett.* **1980**, *74*, 11.
(14) Liou, H. T.; Engelking, P. C.; Ono, Y.; Moseley, J. T. *J. Phys. Chem.*, following article in this issue.
(15) Chang, T.; Li, F. Y. *Appl. Opt.* **1980**, *19*, 3651.
(16) Edwards, J. W.; Kington, G. L. *Trans Faraday Soc.* **1962**, *58*, 1323.

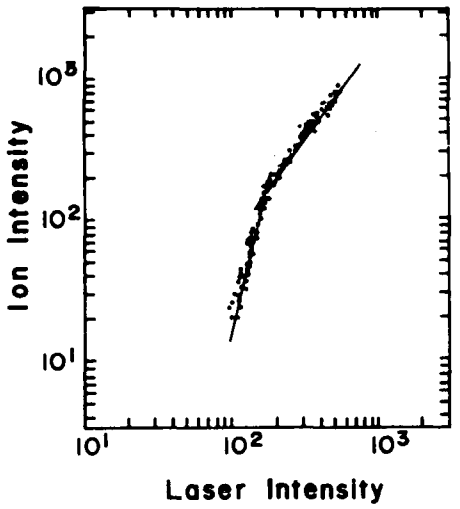

Figure 3. Ion signal vs. laser intensity at 447.6 nm.

beam mode, a Lasertechnics LPV pulsed molecular beam valve, supplied with Ar carrier gas at 1000 Torr and ferrocene at room temperature vapor pressure, provided a source of molecules in a chamber evacuated to 6×10^{-6} Torr by a 6-in. diffusion pump.

Results

The ionization intensities, as functions of the dye laser wavelength, and obtained with 440, 440 + 351, and 440 + 248 nm, are shown in Figure 2.

Dye Laser 440-nm Dissociation. The strong features of the C 440 laser scan are readily assigned to the a^5D_J–e^5D_J two-photon transitions of Fe, using the Fe levels provided by Corliss and Sugar.[17] This is similar to a spectrum previously published by Leutwyler et al.[18] The $\Delta J = 0$ transitions dominate the spectrum in the 447.5–448.3-nm region with five peaks representing J = 0–4. The $\Delta J = \pm 1, \pm 2$ transitions are also present at much lower intensity. Higher laser powers revealed more of the weaker structure and saturated the stronger structure. The smaller peaks in the spectrum can be assigned to either one- or two-photon resonant transitions originating from the ground a^5D multiplet of Fe. Very weak peaks are assigned to transitions originating from the a^5F states. Nearly all of the iron appears as $Fe(a^5D_J)$.

The relative population of the various J states of $Fe(a^5D_J)$ can be estimated by assuming that the $\Delta J = 0$ transitions, for J = 0–4, are saturated at high, constant laser power, and the peak heights represent the populations. The best fit of levels J = 1–4 to a thermal distribution corresponds to a temperature of 1200 K at typical, saturating laser powers of 4 mJ/pulse. The $J = 0$ peak is always anomalously high, possibly due to the overlap with the shoulder of the $J = 1$ peak.

Figure 3 shows the saturation behavior of the $J'' = 4 \rightarrow J' = 4$ line. The low-power slope of 4.4 ± 0.2 indicates a least four photons are rate controlling for the combined process of dissociation followed by ionization. This is understood as second-order photon dependence for molecular dissociation, and second-order photon dependence for the resonant two-photon atomic transition. Saturation of the latter results in a slope of 1.8 ± 0.3 at high powers, controlled by dissociation.

351-nm Dissociation. The 351-nm + C440 two-color spectrum shown in Figure 2b has many features identical with those of the C440 single-color spectrum. Several new peaks detected can be assigned to the resonances in Fe listed in Table I, resulting from transitions driven by the visible radiation either following or preceding transitions driven by the XeF excimer radiation.

Strikingly, the majority of the features do not increase when 351-nm radiation is added to the visible. Thus, most of the signal results from the 440-nm radiation alone. The 351-nm radiation with the photon intensities used in this study does not increase the rate of ferrocene dissociation, nor does it produce new iron states; it only provides additional possibilities for resonant iron atom transitions.

TABLE I: Resonances in the Two-Color Ionization of Fe Involving 351/353-nm Excimer Radiation and the C440 Dye Laser

wavelength, nm	transitions
442.87	$a^5D_3 \rightarrow z^7F_4 \rightarrow e^7G_3$
	$\rightarrow f^5F_4$
	$\rightarrow v^3F_4$
443.64	$a^5D_2 \rightarrow z^7F_1 \rightarrow e^3D_2$
	$\rightarrow f^5F_2$
	$\rightarrow y^1D_2$
	$\rightarrow e^7G_1$
444.67	$a^5D_2 \rightarrow z^7F_2 \rightarrow t^5D_2$
	$\rightarrow u^5P_3$
446.78	$a^5D_1 \rightarrow z^7F_0 \rightarrow f^5F_1$
447.31	$a^5D_1 \rightarrow z^7F_1 \rightarrow e^3D_2$
	$\rightarrow f^5F_2$
	$\rightarrow y^1D_2$
	$\rightarrow e^7G_1$

248-nm Dissociation. Adding 248-nm radiation to that of the C440 dye laser drastically changes the spectrum, as evident in Figure 2c. Even low KrF excimer laser intensity (0.3 mJ/pulse) generates new features that exceed the magnitude of the strong $a^5D_{J'} \rightarrow e^5D_{J'}$ transitions. Furthermore, increasing the 248-nm radiation increases the background ion signal. In addition, some of the resonant transition ion peaks are actually diminished with higher 248-nm intensities.

The resonant transitions of Fe ($a^5D_4 \rightarrow x^5F_4$, $a^5D_3 \rightarrow x^5F_4$) within the KrF laser bandwidth deplete the ground multiplet J = 4 and $J = 3$ level populations. This reduces the intensities of the strong two-photon resonant transitions originating from these levels. Additionally, the x^5F levels ionize in the presence of the strong 248-nm radiation, contributing the strong ionization background. Finally, many of the new transitions originate from higher iron states, particularly the a^3P^0 multiplet.

The ionization background due to 248-nm radiation alone is approximately first order with respect to the photon flux. This is consistent with a mechanism that is saturated in all steps except the first: absorption by ferrocene.

Mass Spectra of Product Ions. A mass spectrum of the MPD/MPI products of ferrocene in the C440 dye region revealed only Fe^+ ions when the pulsed molecular beam configuration was employed, consistent with the work reported by Leutwyler et al.[18] In the static gas cell configuration, $FeCp^+$, $FeCp_2^+$, and Cp^- were observed as well, obviously resulting from secondary collisions. Ion–molecule collisions have similarly accounted for a variety of fragment ions from the MPI of $Fe(CO)_5$.[19] The spectra of each of the ions from ferrocene revealed a structure identical with that of the Fe^+ spectrum, shown in Figure 2a. Fragment ions of the cyclopentadienyl ring were not observed. In contrast to the MPI study by Fisanick et al.,[20] where no benzene was detected from the photodissociation of $Cr(C_6H_6)_2$ and $Cr(CO)_3C_6H_6$, ferrocene has exhibited absorption by the cyclopentadienyl ring after flash photolysis.[21] Mechanisms to account for the various ions detected in this work presume the formation of the cyclopentadienyl free radical from the dissociation of ferrocene. In the two-color MPD/MPI spectra, the same product ions were observed as in the single-color spectrum. The most likely exothermic ion–molecule reactions are the following:

$$Fe^+ + FeCp_2 \rightarrow Fe + FeCp_2^+ \quad (1)$$

$$Fe^+ + Cp + M \rightarrow FeCp^+ + M \quad (2)$$

$$FeCp + e^- \rightarrow Fe + Cp^- \quad (3)$$

$$Cp + e^- + M \rightarrow Cp^- + M \quad (4)$$

(17) Corliss, C.; Sugar, J. *J. Phys. Chem. Ref. Data* **1982**, *11*, 135.
(18) Leutwyler, S.; Even, U.; Jortner, J. *J. Phys. Chem.* **1981**, *85*, 3026.
(19) Whetten, R. L.; Fu, K. J.; Grant, E. R. *J. Chem. Phys.* **1983**, *79*, 4899.
(20) Fisanick, G. J.; Gedanken, A.; Eichelberger, IV, T. S.; Kuebler, N. A.; Robin, M. B. *J. Chem. Phys.* **1981**, *75*, 5215.
(21) Thrush, B. A. *Nature (London)* **1956**, *178*, 155.

The ionization potential is 7.871 eV for Fe,[17] and 6.747 eV for ferrocene.[22] Thus the charge-transfer reaction 1 is exothermic by more than 1 eV. From the relative intensities of the respective ion peaks and considering the distance from the ionization region to the detector entrance (2 mm) and the 7 mTorr of ferrocene, the charge-transfer cross section is estimated to be on the order of 3×10^{-15} cm^2.

Reaction 2 is the only exothermic reaction mechanism forming $FeCp^+$ from a bimolecular collision. This association reaction is only 0.35-eV exothermic, derived from the $FeCp^+$ appearance potential reported by Bar et al.,[22] and subsequent collisions of the complex may serve to stabilize this product ion. Ion–molecule reactions involving Fe^+ with $FeCp_2$ or FeCp to form $FeCp^+$ are endothermic by 3 and 1.3 eV, respectively, from Bar's[22] data, in conjunction with the ferrocene dissociation energy reported by Lewis and Smith.[23] Kinetic shift effects associated with the appearance potential measurement of $FeCp^+$ in ref 22 cannot compensate enough to make these reactions exothermic.

Electrons from the three-photon ionization of Fe at 447.5 mm have less than 0.45 eV of kinetic energy[24] which permits two mechansism for Cp^- formation. Although dissociative electron attachment to ferrocene forming $FeCp + Cp^-$ requires at least 1.7-eV electrons, either the dissociative attachment to FeCp, (3), or the simple association reaction, (4), could account for the negative ion formation. The C_5H_5 electron affinity is 2.21 eV[22] and the energy to dissociate FeCp is also 2.21 eV,[23] thus reaction 3 can occur. Reaction 4 requires either a stabilizing collision or a mechanism to convert the excess energy to vibrations in the C_5H_5 ring in order to prevent detachment.

Discussion

The foremost question that results from this work is why ferrocene MPD is not aided by 351-nm radiation. Several possibilities can be explored.

First, lack of absorption at 351 nm as an explanation may be discarded. The absorption cross section[26,27] is lower by only one order of magnitude from that at 450 nm, and it is unlikely that the second photon absorption process would be forbidden by any more than this. It should also be recognized that we have at least an order of magnitude greater photon flux available at 351 nm, and that the dissociation at 351 nm would proceed in a 1 + 1 process via a known absorption resonance. It is very unlikely that ferrocene is unable to absorb two photons of 351-nm radiation in a two-step process.

One possibility may account for lack of iron production. The ferrocene may quickly equipartition the 0.9-eV excess energy among its vibrational modes, making this energy unavailable for rapid dissociation. Thus, in the case of 351-nm radiation, an RRKM unimolecular decomposition model may apply.

In the case of 351-nm radiation, with 0.9-eV excess energy, a Kassel semiclassical approximation for the RRKM unimolecular decomposition reaction rate is on the order of 10^{-9} s^{-1}. Thus, the decomposition by an RRKM mechanism may be too slow to observe.

One reason a direct dissociation does not occur with 0.9-eV excess energy is that no appropriate singlet energy surface occurs at this energy in the Franck–Condon region. A direct dissociation needs a repulsive electronic surface that correlates to the dissociation products. In a prototype for photodissociation, alkali halide $\tilde{A} \leftarrow \tilde{X}$ absorption[11] occurs between the ionic ground state and the covalent excited state. The dissociation causes a diffuse absorption spectrum. Formally, we have a case of a predissociation, since the $\tilde{A}$ state adiabatic surface correlates to high energy ionic products. However, dissociation occurs through a curve crossing with the nearby $\tilde{X}$ state that does correlate with the correct neutral products. This predissociation occurs rapidly,[28] and might best be viewed as a direct dissociation on a diabatic surface that crosses over to the correct products.

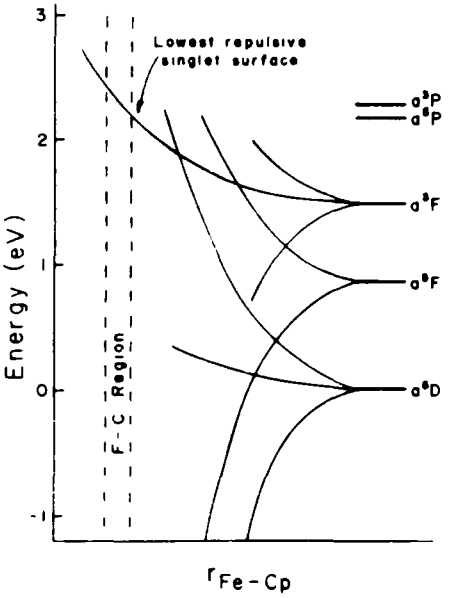

Figure 4. Schematic correlation of the ferrocene states with the Fe + 2Cp dissociation products. The lowest repulsive singlet surface correlates to the a^3F, 1.5 eV above dissocation threshold. Multiple curve crossings to a^5D and a^3F repulsive states occur.

Using this example, we may examine dissociation of ferrocene in a new light. For rapid dissociation to occur, there must be an adiabatic, or a diabatic, repulsive surface in the Franck–Condon region. Although the presence of the high nuclear charge iron atom weakens the spin-selection rules, singlet–triplet photoabsorption processes are at least three orders of magnitude weaker than corresponding singlet–singlet transitions. Thus to be strongly photoactive, the appropriate surface is expected to be a singlet. We notice from Figure 4 that the lowest atomic triplet is the a^3F state 1.5 eV above the ground a^5D state. A singlet ferrocene surface may correlate to a triplet iron plus two doublet cyclopentadienyls, but not to a quintet iron plus two radicals. Thus, the first repulsive singlet surface will be at least 1.5 eV above the dissociation threshold. All these points taken together, we may reach the hypothesis that the active repulsive singlet surface is at least 1.5 eV above the dissociation threshold.

In support of this hypothesis, we note that the known MPD processes rapidly producing iron, whether two photons of wavelengths shorter than 300 nm, or three photons shorter than 450 nm, all provide at least 1.5-eV excess energy. Two photons of 350 nm are insufficient.

It must now be remarked that the actual products appear primarily in quintet states, in addition to appearance in triplet iron states. Curve crossings such as those shown in Figure 4 would have to be responsible. This is not unusual: the determination of the activation energy barrier for ferrocene dissociation, and thus the energy of dissociation of ferrocene itself, depends upon a curve crossing rapid on the time scale of dissociation. The singlet surface provides a terminal state for photoabsorption, and the initial force for separation of the products; the subsequent curve crossings provide access to the final product states.

In contrast to the case of too little energy, less than 1.5 eV, the case of two 248-nm photons would provide ample energy for dissociation, presumably on a higher singlet repulsive surface that correlates to the a^3F or another, higher triplet. Multiple curve crossings provide ample possibilities of product states. Thus it

(22) Bar, R.; Heines, T.; Nager, C.; Jungen, M. *Chem. Phys. Lett.* **1982**, *91*, 440.
(23) Lewis, K. E.; Smith, G. P. *J. Am. Chem. Soc.* **1984**, *106*, 4650.
(24) Nagano, Y.; Achiba, Y.; Sato, K.; Kimura, K. *Chem. Phys. Lett.* **1982**, *93*, 510.
(25) DiDomenico, A.; Harland, P. W.; Franklin, J. L. *J. Chem. Phys.* **1972**, *56*, 5299.
(26) Armstrong, A. T.; Smith, F.; Elder, E.; McGlynn, S. P. *J. Chem. Phys.* **1967**, *46*, 4321.
(27) Sohn, Y. S.; Hendrickson, D. N.; Gray, H. B. *J. Am. Chem. Soc.* **1971**, *93*, 3603.
(28) London, F. *Z. Phys.* **1932**, *74*, 143.

is likely that a number of product states would result, in agreement with the large number of product states observed.

This hypothesis explains the observed facts; it differs from the statistical hypothesis of either RRKM or maximal entropy formulations. The latter do not imply a rapid dissociation, and in fact RRKM implies a relatively slow metastable dissociation, too slow for the production of Fe on the nanosecond time scale.

Several experiments that would distinguish between statistical and direct dissociation may be imagined. One that would be diagnostic would be the characterization of the recoil of the three resulting fragments. A direct dissociation on a repulsive surface would impart significant kinetic energy to at least two fragments. The large kinetic energy of the iron, demonstrated in the subsequent paper, supports this direct dissociation hypothesis.

Conclusions

The MPD products of ferrocene vary as amounts of excess energy increase. With a small 0.9-eV excess, iron atoms are not rapidly produced. With 2.1-eV excess, ferrocene rapidly dissociates, producing iron atoms in predominantly the ground a^5D multiplet. With 3.8-eV excess energy, not only is iron produced rapidly, but the iron appears in a large number of electronic states.

With two wavelengths, the possible MPI resonances increase in number, giving new structural features in an MPI spectrum. 248-nm excimer radiation has a strong resonance with a^5D_3 and a^5D_4 states or iron, leading to efficient ionization via resonant MPD of ferrocene and resonant MPI of iron. One result of this study is that 351-nm radiation does not dissociate ferrocene rapidly and 248-nm radiation does not dissociate ferrocene cleanly. MPD studies with better knowledge of the product Fe states would best be performed using three photons of 440 nm or two photons of 300 nm.

Acknowledgment. This research was supported by the Army Research Office and the Air Force Office of Scientific Research under ARO Contract Nos. DAAG-29-81-K-0117 and DAAG-29-81-K-0154 and by the NSF under Grant No. CHE-8109266. Special thanks to Dan Cowles for initial work on ferrocene, and to Russell Desiderio for useful suggestions for data treatment.

Registry No. Fe, 7439-89-6; ferrocene, 102-54-5.

Reprinted from The Journal of Physical Chemistry, 1986, *90*, 2892

Atomic Iron Recoil in Multiphoton Dissociation of Ferrocene

H. T. Liou,† P. C. Engelking,* Y. Ono, and J. T. Moseley

Departments of Physics and Chemistry, University of Oregon, Eugene, Oregon 97403
(Received: October 11, 1985)

The translational energy of atomic iron, produced by a three-photon dissociation of bis(cyclopentadienyl)iron (ferrocene), has been measured by using the atomic multiphoton ionization Doppler line width at 440 nm. The iron atoms have an appreciable amount of recoil, indicating that the ferrocene dissociation process is nonconcerted and does not preserve a center of symmetry. This is also evidence for a dissociation via one or more repulsive electronic states, rather than by statistical, unimolecular decay of a hot ground state.

Introduction

Many organometallic compounds photodissociate upon absorption of light.[1-7] This process can dominate their photophysics in an intense laser radiation field. In one or several multiphoton dissociation (MPD) steps, a central metal atom can shake off its ligands, leaving it as a bare metal atom. In spite of relatively low ionization potentials for many organometallic compounds, the rate of this MPD often exceeds the rate of direct ionization of the molecule by several orders of magnitude.[8-15]

The metal atoms are detectable by a subsequent resonant atomic multiphoton ionization (MPI) event.[8-14] Because resonant multiphoton ionization can be extremely efficient, an overall MPD/MPI process can dominate direct multiphoton ionization of molecules. This is easily demonstrated in a wavelength scan in a multiphoton ionization experiment: strong features corresponding to wavelengths of atomic absorptions appear in the spectra of organometallic compounds. Figure 1 shows this for ferrocene.

When the dissociating laser is not tuned to an atomic resonance, this process of multiphoton dissociation of a volatile organometallic compound can produce high (ca. 10^{16} cm^{-3}) concentrations of metal atoms in the gas phase. One may imagine a number of uses for optically controllable, local production of high densities of metal atoms. For example, metal mirrors may be plated onto surfaces with micron resolution by multiphoton dissociation of metal alkyls.[16] One goal of investigation into this MPD mechanism is to determine how much control could be exercised over this process of metal atom production. One question immediately stands out: What is the translational temperature of the metal atoms?

When the dissociating laser is tuned to an atomic resonance, a strong ionization, characteristic of a particular element, is observed. Atomic absorptions may serve as very sensitive analytical markers for the presence of organometallic compounds containing a given metal atom. We may envision MPD/MPI as not only a qualitative, but also a quantitative analytical technique. As in any quantitative atomic absorption technique, knowledge of the

† Present address: Department of Chemistry, University of Pennsylvania, Philadelphia, PA 19104

(1) Eyber, G. *Z. Phys. Chem.* **1929**, *14A*, 1.
(2) Thompson, H. W.; Garratt, A. P. *J. Chem. Soc.* **1934**, 524.
(3) Thrush, B. A. *Nature (London)* **1956**, *178*, 155.
(4) Chou, M. S.; Cool, T. A. *J. Appl. Phys.* **1977**, *48*, 1551.
(5) Jonah, C.; Chandra, P.; Bersohn, R. *J. Chem. Phys.* **1971**, *55*, 1903.
(6) Karney, Z.; Naaman, R.; Zare, R. N. *Chem. Phys. Lett.* **1978**, *59*, 33.
(7) Mitchell, S. A.; Hackett, P. A.; Rayner, D. M.; Humphries, M. R. *J. Chem. Phys.* **1985**, *83*, 5028.
(8) Leutwyler, S.; Even, U.; Jortner, J. *Chem. Phys. Lett.* **1980**, *74*, 11.
(9) Leutwyler, S.; Even, U.; Jortner, J. *Chem. Phys.* **1981**, *58*, 409.
(10) Leutwyler, S.; Even, U.; Jortner, J. *J. Phys. Chem.* **1981**, *85*, 3026.
(11) Gedanken, A.; Robin, M. B.; Kuebler, N. A. *J. Phys. Chem.* **1982**, *86*, 4096.
(12) Fisanick, G. J.; Gedanken, A.; Eichelberger, IV, T. S.; Kuebler, N. A.; Robin, M. B. *J. Chem. Phys.* **1981**, *75*, 5215.
(13) Gerrity, D. P.; Rothberg, L. J.; Vaida, V. *Chem. Phys. Lett.* **1980**, *74*, 1.
(14) Engelking, P. C. *Chem. Phys. Lett.* **1980**, *74*, 207.
(15) Duncan, M. A.; Dietz, T. G.; Smalley, R. E. *Chem. Phys.* **1979**, *44*, 415.
(16) Deutsch, T. F.; Ehrlich, D. J.; Osgood, Jr., R. M. *Appl. Phys. Lett.* **1979**, *35*, 175.

0022-3654/86/2090-2892$01.50/0

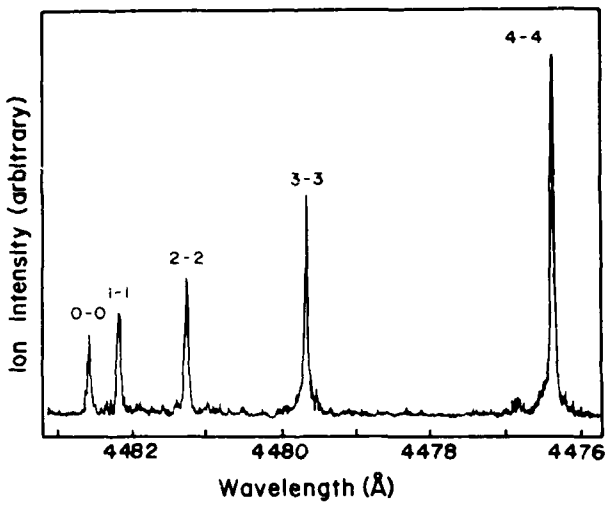

Figure 1. MPD/MPI spectrum of ferrocene in the 448-nm region.

line width is important to correctly match the excitation to the sample. The line width is often dominated by Doppler effects, and again we are led to the question of the translational temperature of the metal atoms.

We have investigated the MPI/MPD of metallocenes and, in particular, ferrocene.[14] In this molecule, the organic ligands face each other with iron between them to form a sandwich compound. Although ample evidence[3,9,10,14,17] indicates that the initial products of photodissociation in the gas phase are iron atom and cyclopentadienyl radicals, the photodissociation of ferrocene is not understood mechanistically. Ferrocene has no observable fluorescence,[18] and electronic excitation might quickly internally convert to a hot ground state. The hot ground state might then pyrolyze, following the unimolecular decomposition kinetics. Another possibility is that ferrocene would lose two cyclopentadienyl ligands in a concerted fashion, as in a repulsive electronic state. Intermediate to these two scenarios is one of sequential loss of ligands through a nonconcerted electronic mechanism, such as established[5] for $Cd(CH_3)_2$.

Each of these choices implies a different kinetic energy distribution for the resulting iron atom. Since the ferrocene molecule has about 25 low-frequency vibrational modes, unimolecular decomposition would result in significant partitioning of the excess energy into vibrations, and only a small amount of translational energy, perhaps only 1/25th of the total available energy, would be expected to appear in iron atom recoil. In this manner, unimolecular decay would produce only a moderately warm distribution of iron atom velocities. In contrast, if the dissociation mechanism were totally concerted, so that a center of symmetry would be retained, the iron atom would be at rest in the center-of-mass system, and would have the velocity of the original ferrocene molecule. Thus, a highly concerted dissociation mechanism would produce cold, possibly even refrigerated, iron atoms. In striking contrast to either of the above mechanisms, if the ferrocene dissociates in a nonconcerted manner via electronically repulsive states, most of the available energy could end up in translational recoil. Since a nonconcerted mechanism no longer requires retention of a center of symmetry, the iron could, possibly, receive a large fraction of the available energy.

The remarkable cleanness of the photodissociation of ferrocene into iron and cyclopentadienyl radicals, as observed in mass spectrometry and electronic spectroscopy, already hints that the dissociation is direct; at least, the dissociation does not occur by pyrolysis from a tightly bound complex. If this latter were the case, one might expect to find significant ring fragmentation of the cyclopentadienyl rings to one, two, and three carbon fragments, or polymerization into ten carbon dimers of the two rings. The lack of either few carbon or ten carbon fragments in either the positive or negative ion mass spectra in the presence of an abundance of cyclopentadienyl radical ions indicates a dissociative mechanism that preserves the ring integrity. This is not always the case for multiphoton dissociation of either organic or organometallic compounds. For example, benzenes and amines are known to extensively fragment under MPI conditions,[19] and this has been interpreted as a highly statistical process involving one or more "hot" intermediates. Likewise, benzene–chromium compounds have been shown to involve benzene ring fragmentation upon MPD.[11,12] From this chemical information, we have already an indication that the dissociation of ferrocene does not involve a pyrolysis of two tightly bound cyclopentadienyl ligands.

This chemical evidence does not rule out a more gentle unimolecular decomposition, one that preserves the ring integrity, but still procedes through a hot ground state. Ferrocene pyrolyzes primarily by whole ring elimination,[20] and a relative, nickelocene, has been found to be the reagent of choice for producing cyclopentadienyl radicals cleanly under flash vacuum pyrolysis conditions.[21] Thus, chemically, it is not possible to rule out a hot unimolecular decomposition as the mechanism of ferrocene photolysis. We need another way to decide between the three alternatives presented above.

In the experiments which follow, the total available energy will be about 2 eV, and the iron is observed to acquire an energy that is a significant part of this. The velocity distribution is characteristic of a temperature more than an order of magnitude above that of room temperature. Thus, measurement of the iron recoil velocity allows us to choose between various dissociation mechanisms, and to decide that the dissociation is nonconcerted, via an electronically excited state.

We have investigated the iron atom recoil in the MPD of ferrocene by monitoring the Doppler line widths of the atomic iron, multiphoton ionization resonances. Although we do not know of previous studies using multiphoton ionization to probe the resonance Doppler profile of a species to obtain translational velocity information, the use of Doppler profiles of laser-induced fluorescence is now well-known.[21-24]

Some caution must be exercised in using resonant MPI to determine Doppler velocities. It must be ensured that the transitions are not broadened by other, electrodynamic effects, such as lifetime broadening or dynamic Stark shifts. Some of the causes for broadening have been pointed out or carefully studied: lifetime shortening,[25] reversals,[26] ac Stark shifts,[27] and recoil.[28] This work gives enough guidance to make a proper choice of transition for the investigation of the Doppler profile.

If a one-photon resonance is followed by a two-photon ionization, the weakness of the latter, nonresonant, multiphoton process requires such high fields that the one-photon resonance is strongly overdriven and dynamically broadened, preventing its use for investigation of the Doppler velocity profile. We have chosen instead a two-photon resonance followed by a one-photon ionization. In this case, the danger is that the upper two-photon resonant state will be lifetime broadened by the rapid ionization by the subsequent one-photon absorption. Thus, it will be necessary to investigate the laser power dependence of the observed line profiles. Nevertheless, this 2 + 1 scheme offers the best possibility of applying MPI to Doppler profile measurements and

(17) Liou, H. T.; Ono, Y.; Engelking, P. C.; Moseley, J. T. *J. Phys. Chem.*, preceding article in this issue.
(18) Sohn, Y. S.; Hendrickson, D. N.; Gray, H. B. *J. Am. Chem. Soc.* **1971**, *93*, 3063.
(19) Bernstein, R. B. *J. Phys. Chem.* **1982**, *86*, 1178.
(20) Hedaya, E. *Acc. Chem. Res.* **1969**, *2*, 367.
(21) Welge, K. H.; Schmiedl, R. In *Laser Induced Processes in Molecules*, Kompa, K. L., Smith, S. D., Eds.; Springer: Berlin, 1979; p 186.
(22) Jhon, M. S.; Dahler, J. S. *J. Chem. Phys.* **1978**, *69*, 819.
(23) McDonald, J. R.; Miller, R. G.; Baronavski, A. P. *Chem. Phys. Lett.* **1977**, *51*, 57.
(24) Drozdoski, W. S.; Baronavski, A. P.; McDonald, J. R. *Chem. Phys. Lett.* **1979**, *64*, 421.
(25) Johnson, P. M. *Acc. Chem. Res.* **1980**, *31*, 20.
(26) Rothberg, L. J.; Gerrity, D. P.; Vaida, V. *J. Chem. Phys.* **1981**, *75*, 4403.
(27) Li, L.; Yang, B.-X.; Johnson, P. M. *J. Opt. Soc. Am. B* **1985**, *2*, 748.
(28) Shirley, J. H. *J. Phys. B* **1980**, *13*, 1537.

avoiding the myriad of other well-known effects that cause line broadening of MPI resonances. In fact, this 2 + 1 scheme is the very basis for a proposed secondary wavelength standard at the 1-MHz level of precision.[29,30]

All line widths and frequencies will be reported at fundamental, one-photon wavelengths. The linear scaling of the Doppler shift with frequency allows us to analyze the velocity shift at the fundamental laser frequency, while the actual two-photon resonance has the Doppler shift of twice this magnitude at the energy of twice the laser frequency. To avoid any confusion, all line widths and shifts will be reported as observed, at the fundamental laser frequency.

This fact, that the resonance is at twice the laser frequency and occurs as a two-photon process, is possibly to our advantage in relaxing the constraints placed upon the line width of the laser used to probe the iron atom Doppler profile. Ideally, if one assumes that the fluctuations at one frequency are uncorrelated to fluctuations at another, the laser profile at the fundamental frequency should be convolved with itself to give the effective two-photon profile at twice the laser frequency. If a Gaussian profile is assumed, the effective width is $(2)^{1/2}$ times broader than the original Gaussians. Projecting this back to the fundamental frequency of the laser, one finds that this appears as a width of $(2)^{-1/2}$, about 30% narrower than the original laser line profile.

It is not wise to depend upon this narrowing. Elliot et al.[31,32] have carefully investigated experimentally the two-photon absorption widths for various types of laser fields. They show that if the laser fluctuations are temporally correlated across the laser frequency profile, the two-photon absorption width can be significantly broader than that given by convolution, which assumes an uncorrelated laser spectrum. This is in accord with the models of Mollow,[33] Agerwal,[34] Alber and Zoller,[35] Zoller and Lambropolous,[36] and Yeh and Eberly,[37] who find that generally, for an n-photon absorption by a "chaotically" amplitude modulated single frequency mode, the width is n times that of the laser. At the frequency of the laser, it appears to have the width of the laser itself.

We have observed two-photon resonances in other systems, such as NO,[38] that are significantly narrower than reported here, and confirm that the laser-limited two-photon line widths are narrower than we require, and that these rather special temporal correlations do not give anomalously wide two-photon absorption profiles here. To be conservative, we will assume that the limiting two-photon absorption is twice the fundamental line width, appearing as the laser width itself at the laser fundamental, and we will not rely upon the thirty percent narrowing expected for a totally uncorrrelated Gaussian frequency spectrum.

Experimental Section

The iron atom recoil is monitored by measurement of the Doppler line profile of a two-photon resonance, a^5D_4–e^5D_4, followed by a nonresonant single-photon ionization of the e^5D_4 state. The iron atoms are generated in the multiphoton dissociation of ferrocene in a three-photon dissociation, using the same 447.65-nm radiation that probes the iron atoms.

The experimental setup has been described in ref 38. Briefly, two parallel stainless-steel plates, supplied with a difference in potential of 200 V, collect the total ions in a static cell at 100-mtorr pressure. Slow pumping removes reaction products.

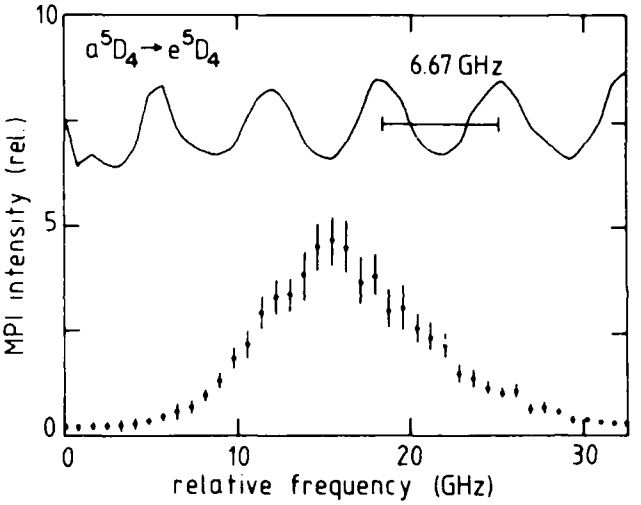

Figure 2. A line profile of the Fe a^5D_4–e^5D_4 resonantly enhanced MPI signal at a moderate power level. A 6.67-GHz free spectral range etalon calibrates the laser frequency. The laser line width is about 3 GHz. The 10-GHz broadening results from both a Doppler component, observable at low powers and a Lorentzian, power-dependent component. At this power, the Lorentzian dominates. The asymmetry is ascribed to a weaker, nearby transition, at about 26 GHz on this scale.

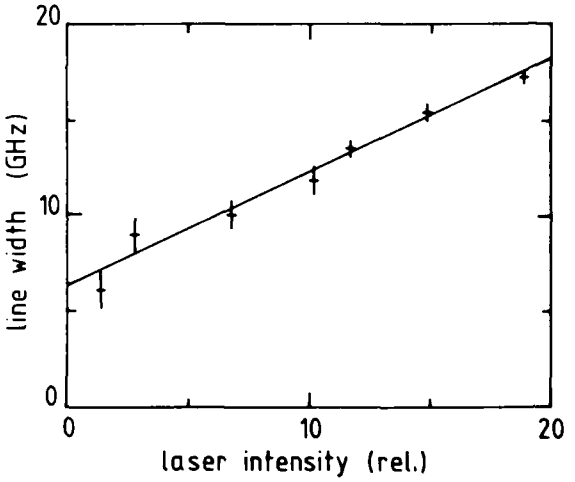

Figure 3. A plot of observed line width vs. laser intensity. The laser energy varies between 0 and 8 mJ per pulse, weakly focused with a long focal length lens. Two components contribute to the line width: a low power residual width from the convolution of the laser line with the Doppler line shape, and a power broadening component. The combined effect gives an almost linear power dependence.

A laboratory computer accumulates data (ionization current vs. wavelength), monitors the laser intensity, and records the intensity pattern of a transmission etalon. The 6.67-GHz free spectral range of the etalon transmission calibrates the wavelength scan of the laser.

The laser oscillator's configuration is similar to that of Chang and Li.[39] We maintain stable operation and easy alignment by replacing the total reflector end mirror with a wedge output coupler[40] rather than using the grating for output. Maximum energy of the laser after one stage of amplification is 8 mJ per pulse, with a stable, power-independent line width of 2.93 GHz.

At resonance, the MPI signal shows a roughly fourth-order power dependence, which becomes roughly second order at high powers. This is consistent with our previous work in ferrocene.[17] At low powers, the fourth-order dependence corresponds to second-order dissociation and second-order MPI; the ionization of the excited iron atom is saturated. At high powers, the dissociation

(29) Hall, J. L. *Science* **1978**, *202*, 147.
(30) Lee, S. A.; Helmcke, J.; Hall, J. L.; Stoicheff, B. P. *Opt. Lett.* **1978**, *3*, 141.
(31) Elliot, D. S.; Hamilton, M. W.; Arnett, K.; Smith, S. J. *Phys. Rev. A* **1985**, *32*, 887.
(32) Elliot, D. S.; Hamilton, M. W.; Arnett, K.; Smith, S. J. *Phys. Rev. Lett.* **1984**, *53*, 439.
(33) Mollow, B. R. *Phys. Rev.* **1968**, *175*, 1555.
(34) Agerwal, G. S. *Phys. Rev. A* **1970**, *1*, 1445.
(35) Abler, G. H.; Zoller, P. *J. Phys. B* **1980**, *13*, 4567.
(36) Zoller, P.; Lambropoulos, P. *J. Phys. B* **1980**, *13*, 69.
(37) Yeh, J. J.; Eberly, J. *Phys. Rev. A* **1981**, *26*, 888.
(38) Steimle, T. C.; Liou, H. T. *Chem. Phys. Lett.* **1983**, *100*, 300.
(39) Chang, T.; Li, F. Y. *Appl. Opt.* **1980**, *19*, 3651.
(40) Lumonics, Ltd., 105 Schneider Rd., Kanata, Ontario, Canada.

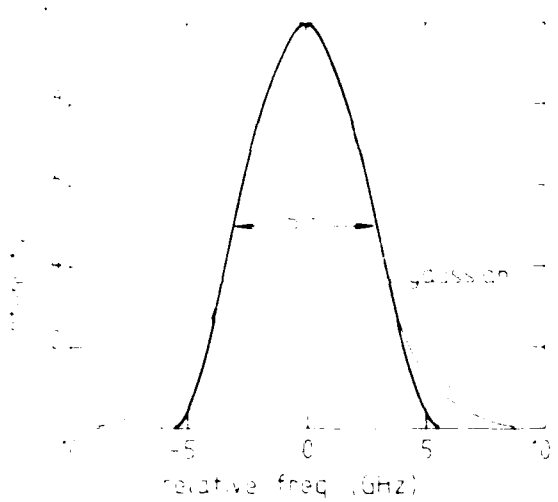

Figure 4. Theoretical model of the line shape assuming equipartition of 2.1 eV into recoil of three fragments Fe + 2Cp. Compared is the line profile of a Gaussian distribution of the same width. The three-body equipartition line shape lacks the wings exhibited by the Gaussian.

is saturated. At any given power level, the signal is proportional to the amount of iron produced in the a^5D_4 state by dissociation.

To obtain the MPI line shape, the laser wavelength is scanned over the entire resonant transition by tuning the grating. This is repeated at various laser powers. The results of one run at one laser intensity are shown in Figure 2.

Results

Figure 3 shows a plot of multiphoton ionization line width vs. laser intensity. Two effects are observable. First, the intercept at zero laser power is significantly wider than the line width of the probe laser, which was 2.93 GHz. Second, although the laser line width does not vary with the laser power (as confirmed by measurement using an etalon), the multiphoton ionization line width does vary with power.

The broadening of the multiphoton ionization resonance at low laser intensities is attributed to the Doppler effect of the iron recoil. The laser line width was measured to be 2.93 GHz. When this is deconvoluted from the observed intercept width of 6.0 ± 0.8 GHz, a resulting width of 5.2 ± 0.8 GHz remains. The half-width corresponds to a velocity representing 0.4 ± 0.1 eV of energy in the iron atom motion. The average energy of the iron atoms, assuming an isotropic velocity distribution, is 0.7 ± 0.2 eV. Thus, it is immediately evident that the iron atoms have a significant amount of translational energy imparted to them by the dissociation event.

The increase in line width with laser power reflects the expected power broadening of the multiphoton event. The two-photon resonance a^5D_4–e^5D_4 is followed by very rapid one-photon ionization. This rapid ionization of the e^5D_4 state causes lifetime broadening. (The power dependence of this process is second-order overall, explained by a rate-limiting two-photon resonance followed by a rapid, one-photon ionization.) A moderate ionization cross section of 10^{-20} cm^{-2} for the e^5D_4 state is consistent with this magnitude of lifetime broadening of the e^5D_4 state.

Another piece of evidence points to lifetime broadening as the cause of the power dependence of the line width. Lifetime broadening would appear as a Lorentzian component to the line shape. A rough deconvolution of the line shape into a Gaussian and a Lorentzian (based on the Voigt profiles given by Davies and Vaughn[41]) shows a broadening of the Lorentzian component with laser power, while the Gaussian component remains constant.

This analysis also shows that the intercept of the Lorentzian component at low powers is negative, while the constant Gaussian Doppler width is too large. These spurious effects, produced by forcing the line shape to a Voigt profile, can be accounted for by an iron velocity profile that has less intensity in its wings than a Gaussian would have.

Discussion

The dissociation threshold of ferrocene into two radicals and atomic iron occurs at about 6.2 eV.[42] Thus, with three photons of 447.5 nm (8.31 eV), 2.1 eV is available for dissociation. If all of this energy appeared in translation, the maximum energy available to the iron, based on energy and momentum considerations, would be 1.48 eV.

If the energy available for dissociation is equipartitioned into isotropic recoil of Fe and cyclopentadienyl fragments, the line shape should have the form $(x^2 - x^2_{max})^2$, where x = frequency shift, and x_{max} = 5.1 GHZ. The fwhm for a line of this shape is 1.08 x_{max} or, in this case, 5.5 GHz. This should be compared to the Doppler line width observed here: 5.2 ± 0.8 GHz. Thus, the line widths observed here are consistent with most of the excess energy appearing in recoil of the fragments and with very little correlation of the direction of recoil of the two ligands.

Another way of looking at this energy partitioning is to recognize that if the 2.1 eV is divided up among the three almost equal mass fragments, Fe + 2Cp, one third, or 0.7 eV, should be allotted each fragment on the average. This agrees with the average energy of 0.7 ± 0.2 eV we obtain assuming an isotropic Fe recoil.

The maximum energy restriction leads to the observed line shapes. Comparison of an equipartition line shape to that of a Gaussian of the same width reveals that the Gaussian would have an intensity of 0.1 at x_{max}. Thus, energy and momentum restrictions cut off the wings of an otherwise Gaussian distribution and appear to square up the line profile. This corresponds approximately to what is observed.

The actual magnitude of the line width must not be over interpreted. We have assumed ejection of iron nonpreferentially with respect to the direction of light propagation but have not demonstrated this. This unknown angular dependence has prevented us from carefully analyzing the line shapes to extract the details of the iron atom energy distribution. We can, however, remark on the overall nature of the angular distribution, and put some bounds on its asymmetry. If the iron were preferentially ejected along the polarization axis, perpendicular to the light propagation direction, we would severely undercount the fast iron atoms. Since we actually observe close to the maximum available energy for translation, this cannot be the case. Instead, it is possible that iron is ejected preferentially perpendicular to the polarization axis. In this case, we would have overestimated the population of fast iron; in the extreme, we would have overestimated the energy width by a factor of about two.

The large amount of kinetic energy observed in this experiment correlates well with the total amount of excess energy available in a three-photon (two + one) absorption, as calculated from the dissociation energy of ferrocene of 6.2 eV.[42] This number has recently been questioned, as discussed by Bar et al.[43] They rationalize that the dissociation energy could be as high as 7.8 eV. Yet, this would be inconsistent with the amount of kinetic energy release we observe, and we view this unlikely. Thus, this work is consistent with a ferrocene dissociation energy of about that others report: 6.2 eV.

We should also point out what this experiment does not prove. It is not yet established whether the third photon is absorbed before or after second ligand departs. On the face of it, our evidence for a nonconcerted mechanism might be taken to indicate that, after the first two photons are absorbed, partial dissociation occurs, in which one ligand departs. Based upon a simple, additive model of bonding, we might imagine that each ligand has 6.2/2 = 3.1 eV bond energy, and two photons might strip off one ligand. There is yet little evidence to support this.

(41) Davies, J. T.; Vaughn, J. M. *Astrophys. J.* **1963**, *137*, 1302.

(42) Muller, J.; D'Or, L. *J. Organometal. Chem.* **1967**, *10*, 313. Wilkinson, G.; Pauson, P. L.; Cotton, F. A. *J. Am. Chem. Soc.* **1954**, *76*, 1970. Conner, J. A. *Top. Current Chem.* **1977**, *71*, 72.

(43) Bar, R.; Heines, T.; Nager, C.; Jungen, M. *Chem. Phys. Lett.* **1982**, *91*, 440.

Bonding in organometallic compounds is not additive: the removal of the first ligand requires much more energy than the removal of subsequent ligands. This is seen in the relative bond strength in carbonyls,[44] and in the relative bond strengths of metallocene cations.[45] In the ferrocene cation, appearance potentials[45,46] indicate it takes five to fifteen times as much energy to remove the first ligand as it does to remove the second ligand, which may have a bond strength as low as a third of an electronvolt. In ferrocene itself, this disparity of bond strengths is also expected, since the neutral iron with two ligands has a $(e_g)^4(a_{1g})^2$ d electron configuration, while the metal with only one ligand has a $(e_g)^4(a_{1g})^1(e_u)^1$ d-electron configuration. Removal of one ligand requires the promotion of an electron. This is the reason that the isoelectronic cobaltocene cation, with the same electronic configuration, has the highest first ligand dissociation energy of all the first transition-metal-row metallocene cations: 2.8 eV.[45] Ferrocene pyrolysis kinetics[20] suggests an energy for loss of a single ligand by ground-state ferrocene of 4.0 eV, implying a second ligand dissociation energy of 2.1 eV. Thus, for the ferrocene ground state, the first dissociation requires almost twice as much energy as the second. While numerically this implies that there is thermochemically enough energy in two photons to remove one ligand from ground-state ferrocene, it is not yet demonstrated that this dissociation of photoexcited ferrocene will, in fact, occur before absorption of an additional photon. Thus, it is quite possible that the kinetics require absorption of all three photons before any dissociation actually occurs.

Finally, this work should be placed in the context of what is already known about photodissociation. As in a direct photodissociation such as illustrated by CH_3I into $CH_3 + I$ studied by Riley and Wilson,[47] most of the energy partitioning is into translation, rather than into vibrations. This is taken as evidence that the dissociation occurs by excitation to a steep, dissociating electronic surface, on which dissociation takes place without significant time for equipartitioning the energy into various internal modes of the fragments. Rapid photodissociation of metal alkyls has also been observed: Jonah et al.[5] and Tamir et al.[48] have investigated the angular distributions of the three fragments of $Cd(CH_3)_2$. Significant anisotropies of all fragments are observed. This would be inconsistent with a simple unimolecular decay model, and these authors find their results consistent with a model that rapidly ejects the two ligands, not together, but in rapid succession. It is this type of model that we also favor for the dissociation of ferrocene.

Conclusion

Ferrocene undergoes multiphoton dissociation in a nonconcerted manner that efficiently delivers recoil energy and momentum to the central iron atom. The Doppler width of the atomic absorptions is predicted by a simple model assuming equipartition of the excess energy among the translational degrees of freedom. These results point to a dissociative mechanism via repulsive electronic states.

Acknowledgment. This work has been supported by the Army Research Office under Contract Nos. DAAG-29-81-K-0154 and DAAG-29-81-K-0117 and by the NSF under Grant No. CHE-8109266.

Registry No. Ferrocene, 102-54-5; Fe, 7439-89-6.

(44) Engelking, P. C.; Lineberger, W. C. *J. Am. Chem. Soc.* **1979**, *101*, 5569.
(45) Cais, M.; Lupin, M. S. *Adv. Organometal. Chem.* **1970**, *8*, 211.
(46) Puttermans, J. P.; Hanson, A. *Ing. Chim. (Brussels)* **1971**, *53*, 17.
(47) Riley, S. J.; Wilson, K. R. *Faraday Discuss. Chem. Soc.* **1972**, *53*, 132.
(48) Tamir, M.; Halava, U.; Levine, R. D. *Chem. Phys. Lett.* **1974**, *25*, 58.

END
DATE
FILMD
3-88
DTIC